Accepted Manuscript

Antileishmanial activity of quinazoline derivatives: Synthesis, docking screens, molecular dynamic simulations and electrochemical studies

Cesar Mendoza-Martínez, Norma Galindo-Sevilla, José Correa-Basurto, Victor Manuel Ugalde-Saldivar, Rosa Georgina Rodríguez-Delgado, Jessica Hernández-Pineda, Cecilia Padierna-Mota, Marcos Flores-Alamo, Francisco Hernández-Luis

PII: S0223-5234(14)01160-X

DOI: 10.1016/j.ejmech.2014.12.051

Reference: EJMECH 7611

To appear in: *European Journal of Medicinal Chemistry*

Received Date: 27 August 2014

Revised Date: 23 November 2014

Accepted Date: 28 December 2014

Please cite this article as: C. Mendoza-Martínez, N. Galindo-Sevilla, J. Correa-Basurto, V.M. Ugalde-Saldivar, R.G. Rodríguez-Delgado, J. Hernández-Pineda, C. Padierna-Mota, M. Flores-Alamo, F. Hernández-Luis, Antileishmanial activity of quinazoline derivatives: Synthesis, docking screens, molecular dynamic simulations and electrochemical studies, *European Journal of Medicinal Chemistry* (2015), doi: 10.1016/j.ejmech.2014.12.051.

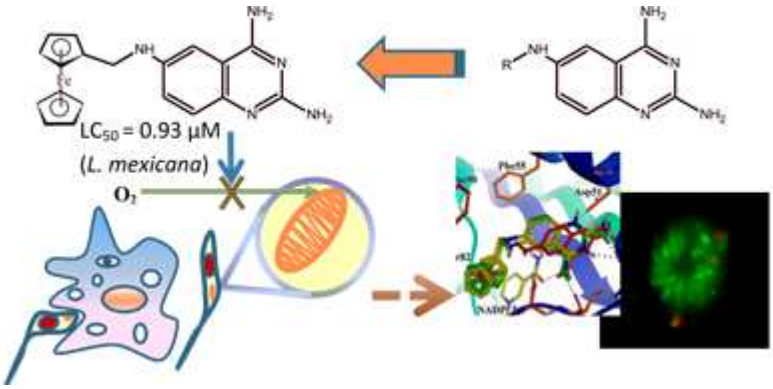

Antileishmanial activity of quinazoline derivatives: Synthesis, docking screens, molecular dynamic simulations and electrochemical studies

Cesar Mendoza-Martínez[1,2], Norma Galindo-Sevilla[3], José Correa-Basurto[4], Victor Manuel Ugalde-Saldivar[5], Rosa Georgina Rodríguez-Delgado[6], Jessica Hernández-Pineda[3], Cecilia Padierna-Mota[7], Marcos Flores-Alamo[6], Francisco Hernández-Luis[2*]

[1]*Programa de Maestría y Doctorado en Ciencias Químicas, Universidad Nacional Autónoma de México, México, DF 04510, México*
[2]*Departamento de Farmacia,* [5]*Departamento de Química Inorgánica y Nuclear,* [6]*Facultad de Química, Universidad Nacional Autónoma de México, México DF 04510, México*
[3]*Departamento de Infectología, Instituto Nacional de Perinatología, México DF 11000, México*
[4]*Escuela Superior de Medicina, Instituto Politécnico Nacional, México DF 11340, México*
[7]*Laboratorio de Especialidades Inmunológicas S.A. de C.V., México DF 07580, México*

*Corresponding author: Tel +525 56225287, *E-mail address*: franher@unam.mx

ABSTRACT

A series of quinazoline-2,4,6-triamine were synthesized and evaluated in vitro against *Leishmania mexicana*. Among them, N^6-(ferrocenmethyl)quinazolin-2,4,6-triamine (**H2**) showed activity on promastigotes and intracellular amastigotes, as well as low cytotoxicity in mammalian cells. Docking and electrochemical studies showed the importance of both the ferrocene and the heterocyclic nucleus to the observed activity. **H2** is readily oxidized electrochemically, indicating that the mechanism of action probably involves redox reactions.

Keyboard: *Leishmania mexicana*; quinazoline; antiprotozoan activity

1. Introduction

The search for antiparasitic molecules has recently become important because of the emergence of drug resistant strains, the toxicity of the known molecules, increased poverty and the percentage of the affected population [1]. Parasitic tropical diseases affect hundreds of millions of people worldwide, however, it has been neglected to develop drugs against these diseases because they primarily affect people in poor regions of the world [1]. Leishmaniasis, African trypanosomiasis, and Chagas disease are vector-borne diseases caused by parasites of the kinetoplastida order [2]. Leishmaniasis is a set of devastating diseases caused by the obligate intracellular protozoa parasites of the *Leishmania* genus, which are transmitted by a group of 50 species and subspecies of phebotomine insects. About 1.5 million of new cases of cutaneous leishmaniasis and 500 000 new cases of visceral disease occur each year. Cutaneous leishmaniasis is endemic in more than 70 countries worldwide [3]. A major emerging problem is co-infection of *Leishmania* with human immunodeficiency virus, especially because there is no effective treatment for these patients [3]. Conventional chemotherapy relies on multiple parenteral administrations of pentavalent antimonials that are considerably toxic and induce resistance. Second-line drugs, such as amphotericin B and its lipid formulations, are either too toxic or too expensive for routine use in developing countries [4]. Recently, miltefosine, a phosphocholine analogue originally developed as an anticancer agent, was introduced as a drug against visceral leishmaniasis, but its effectiveness has still not been conclusively determined and there have already been reported cases of resistance [5]. Because chemotherapy for leishmaniasis is still inefficient, there is an urgent need for the development of new efficient and safe drugs.

In order to find new drugs against leishmaniasis, the computational design of new drugs against parasites has been based on the knowledge and availability of new information from molecular targets [7,8]. With the goal of following this strategy, we chose pteridine reductase (PTR) as the target of the study, which is a protein that appears to be important to the resistance mechanism of *Leishmania*. This enzyme is NADPH-dependent with oxide reductase activity, and pterins are its natural substrate [7]. However, under conditions of cellular stress or when folate metabolism is brought down by molecules that inhibit dihydrofolate reductase (DHFR), PTR may reduce folate, therefore allowing the production of DNA through the salvage route, causing parasite resistance [9-11]. New approaches in the design of antifolates should consider the importance of PTR to discover new molecules capable of inhibiting DHFR and/or PTR through rational design [7].

The isoform PTR1 of *Leishmania major* was co-crystallized with quinazoline-2,4,6-triamine (**TAQ**) [12]. By analyzing the interactions of **TAQ** with the active site of PTR1, the chemical modification of **TAQ** at position 6 was considered because the reception site near this position is large and possesses both polar and non-polar regions (Figure 1). Berman and co-workers, showed the importance of the lipophilic substituents at position 6 of the quinazoline ring, decreasing the ED_{50} against *L. major*. In addition, they have shown that, by increasing the size of the substituent, the ED_{50} increased [13]. In this case, the selection of the chemical substituent at position 6 was based on its potential to function as an anti-protozoal scaffold. With this in mind, nitrobenzene, ferrocene, benzimidazole, anisole and phenol moieties were selected as the substituents in **H1**, **H2**, **H3**, **H4** and **H5**, respectively (Table 1). Ferrocene is present in ferroquine, an anti-malarial drug that is currently under clinical evaluation and has

got a great potential [14]. A number of studies have shown that the introduction of the ferrocene core may significantly enhance the molecule's (desirable) bioactive properties. The ferrocene unit might act as a hydrophobic spacer and/or lipophilicity/bioavailability enhancer (enabling an easier way through cell membranes) [15]. It is also known that ferrocene Fe^{+2}/Fe^{+3} redox chemistry might contribute to the bioactivity of ferrocene derivatives [16]. Benzimidazole is a privileged structure in antiparasitic molecules [17]; particularly, in a compound prepared in our group, 5,6-dicloro-2-(trifluoromethyl)-1*H*-benzimidazole, denoted in this work as **G2** [18]. Nitrobenzene, anisole and phenol groups are present in several anti-parasitic drugs [19, 20].

With the aim of exploring PTR1 binding site surfaces of the protein, we employed docking studies using **TAQ** as ligand and attempted to reproduce this ligand is in the previously reported crystal structure [12]. Next, we performed a molecular coupling of the proposed molecules (**H1–H5)** into active site of *Leishmania* PTR1 and DHFR. The affinity of all the target compounds to both enzymes was higher than the affinity of **TAQ**. Subsequently, the proposed compounds were synthesized and once their structure was elucidated by x-ray crystallographic, they were tested in vitro against the promastigote form of *L. mexicana*. The most active was **H2**. For this reason, chemical modifications were carried out to the **H2** structure (Figure 2) in order to explore changes in biological responses that could cause these structural modifications. Finally, the reduction potential for this group of compounds was carried out using DMSO as aprotic solvent. The data in aprotic solvent did not only describe the situation in that way but it also allowed us to obtain biological significance of interpretation.

2. Results and discussion

124 *2.1.Chemistry*

125 Compounds **H4** and **H5** were first synthesized and evaluated as antichagasic and
126 antiplasmodial agents by Davoll, and co-workers [21]. Since they were not evaluated
127 against *Leishmania*, these molecules were synthesized in this work in order to explore their
128 biological activity against *L. mexicana*.

129 All the **TAQ** derivatives were synthesized according to the route outlined in Scheme 1. The
130 antiprotozoal compound **G2** (5,6-dicloro-2-(trifluoromethyl)-1*H*-benzimidazole) was
131 prepared in our laboratory using known procedures [18]. As shown in Scheme 1,
132 nucleophilic substitution of the bromine atom in 2-bromo-1,1-diethoxyethane by **G2**
133 afforded 5,6-dichloro-1-(2,2-diethoxyethyl)-2-(trifluoromethyl)-1*H*-benzimidazole (**1**).
134 Treatment of **1** with boron tribromide (BBr_3) followed by hydrolysis gave [5,6-dichloro-2-
135 (trifluoromethyl)-1*H*-benzimidazole-1-yl]acetaldehyde (**2**). Preliminary attempts to obtain
136 the aldehyde group with hydrochloric acid [22], I_2/acetone [23] and $FeCl_2$ [24] were
137 unsuccessful. The cyclocondensation of commercially available 5-nitroanthranilonitrile
138 with guanidine hydrochloride yielded 6-nitroquinazoline-2,4-diamine (**3**), which was
139 treated with acetic anhydride followed by hydrogenation under a hydrogen atmosphere
140 using palladium on charcoal to yield *N*,*N*'-(6-nitroquinazoline-2,4-diyl)diacetamide (**4**).
141 Subsequent condensation of **4** with the corresponding aldehyde gave the imine derivatives.
142 The imine group was reduced with sodium borohydride ($NaBH_4$) to yield the proposed
143 molecules (**H1**–**H5**).

144 Of all the compounds synthesized only **H2** gave crystals adequate to carry out an single-
145 crystal X-ray analysis. These studies revealed that **H2** in ethanol crystallizes in the triclinic
146 space group P-1. A view of **H2** is presented in Figure 3, and selected bond distances and
147 torsion angles are listed in Table 2. The asymmetric unit of the **H2** compound consists of

N^6-(ferrocenylmethyl)quinazolin-2,4,6-triamine and three ethanol solvate molecules in general positions. The quinazolin-2,4,6-triamine shows planarity with a *rms* deviation of the fitted atoms of 0.0265. The C2-C1-C19-N1 (106.47°) and C5-C1-C19-N1 (70.20°) torsion angles show a nearly perpendicular arrangement between the ferrocenyl and quinazoline groups.

In the crystal lattice, the neutral ferrocenyl complex and the ethanol solvate molecules participate in multiple hydrogen bonding interactions, such as N-H···O, N-H···N and O-H···O (Figure 4). The majority of the hydrogen bond distances range from 1.87-2.25 Å (Table 3). The interaction between the nitrogen donor atom (N4) and the acceptor atom (N2) forms the $R^2_2(8)$ motif, whereas the N1-H1F···O1C hydrogen bond shows the $D^3_3(17)$ motif. All of these interactions are present in the three crystalline axes and favor three-dimensional growth.

In order to determine the part of the molecule that provides the anti-*Leishmania* effect when quinazoline or ferrocene are used, a series of ferrocene derivatives (**HO2**, **HO4**, **H2A**, **FBC**) were synthesized via reductive amination with varying reagents (Scheme 2).

The structures of all the compounds synthesized were characterized by spectroscopic and spectrometric data. In the ^{1}H NMR spectra of the title compounds, the doublet in the range 4.5–3.9 ppm, integrating for two protons, confirmed the presence of methylene linking the substituent to quinazoline nucleus; whereas in the ^{13}C NMR spectra, the same signal of the secondary carbon of the methylene was seen at δ value of 46 ppm. For the same group of compounds, the signal of proton of the NH exocyclic at position 6 was recorded as triplet at δ values in the region 6–5 ppm. For **H2**, **HO4**, **HO2**, **H2A** and **FBC**, typical ferrocene signals were showed in the region of 4.3– 4.0 ppm in the ^{1}H NMR spectra, and 60–90 ppm

in the ^{13}C NMR spectra. For those compounds having exocyclic amines groups at position 2 and 4 of quinazoline nucleus, the signal derived from two protons was observed at δ values 5.6 and 7.0 ppm, respectively. Regarding ^{1}H NMR spectra of **HO2** and **HO4**, the exocyclic amine group, at position 4 and 2, presented a signal to 7.73 and 5.91 ppm, respectively. Finally, in the downfield region of the same spectrum, the signal of one proton at 10.44 (**HO2**) and 10.78 (**HO4**) ppm revealed the presence of endocyclic NH of quinazoline moiety, suggesting the presence of carbonyl group at position 2 and 4, respectively. This suggestion was supported by IR spectra of both compounds, which exhibited stretch carbonyl characteristic band at 1624 and 1644 cm^{-1}, respectively. Additionally, energetic stability studies confirmed that the most stable tautomers (Gibbs energy of 0 Kcal) for both molecules are those having the carbonyl group. All these data indicate that in **HO2** and **HO4** the C-O bond is present as carbonyl group and the most stable tautomeric form should be as proposed (Figure 5).

2.2.Modeling studies

With the purpose of estimating the interactions of the synthesized compounds with PTR and DHFR, the affinity to both enzymes was analyzed in a theoretical docking study. The crystal structure of tcDHFR (*Trypanosoma cruzi* dihydrofolate reductase ID-PBD: 2H2Q) was used to construct a homologous enzyme, *L. major* was used as a model for *L. mexicana*. The DHFR sequence in *L. mexican*a is unknown; however, the three species (*T. cruz*i, *L. major* and *L. mexicana*) are evolutionarily very close. The molecular dynamics protocol was applied to relax the built protein, and a snapshot at 10 ns was obtained for the docking of all the molecules. The root media square deviation (RMSD) and the radius of gyration (RGyr) indicated that the protein reached convergence (Figure 6). The crystal

194 structure of *L. major* pteridin reductase (1 ID-PBD: 1WOC) was obtained from the Protein
195 Data Bank, and molecular docking was performed with this protein.
196 The free energy analysis of the molecular interaction between the **TAQ** derivatives and the
197 DHFR and PTR1 enzymes showed that all of the compounds bind more strongly to the
198 receptor site than **TAQ**, and the mode of binding was very similar (Figure 7). In the case of
199 the ferrocene derivatives (**HO2**, **HO4** and **H2A**), the differences in the interaction energies
200 were a result of the substituents at positions 2 and 4 (Table 5). For this study, the stability
201 of the different tautomers of **HO2** and **HO4** was analyzed (Figure 5) with the intention of
202 using only the most stable.
203 *2.3. Biological activity*
204 Obtained compounds were tested in vitro against promastigotes form of *L. mexicana*.
205 Initially, the compounds were incorporated into the media at 100 μM and their ability to
206 inhibit growth of the parasite was evaluated in comparison to the control (no drug added to
207 the media). Glucantime was used as the leishmanicidal of reference; pyrimethamine and
208 trimetoprim were used as DHFR inhibitors models. Subsequently, the IC_{50} (50% inhibitory
209 growth concentration) concentration was determined. With exception of **H2** and **H4**, all
210 compounds resulted with poor or null activity (Table 6). Compound **H2** was the most active
211 (IC_{50} = 0.93 μM); the second place went to **H4** (IC_{50} = 14.59 μM). The components of **H2**
212 (ferrocene and **TAQ**) had a poor antileishmanial activity individually. Interestingly, **H2**
213 showed antiparasitic activity from the first hour of being in contact with the parasites. This
214 behavior may be due to the ferrocene moiety contributes with its lipophilicity and redox
215 properties. On the other hand, with exception of **H4**, **FBC** showed slightly higher activity
216 than the quinazoline derivatives, despite having only one phenyl group attached to

ferrocene unit. In **H2**, the **TAQ** portion was necessary for leishmanicidal activity because when the 2- and 4-positions were modified by acetylation (**H2A**) or substitution of the NH_2 group (**HO2**, **HO4**), the activity was lost (Table 6). In the light of these results, only **H2** was selected for the following studies in order to gain an understanding of its biological activity.

There is no obvious correlation with the solubility, however, the solubility of **H2** is greater than ferrocene alone and less than triaminquinazoline. This, of course, could be a cause of antileishmanial activity shown because ferrocene is dissolved in greater amounts. However, **H2A** is much more soluble than most derivatives (except **TAQ**, which is extremely soluble) but this is not enough to improve the activity, so, that interaction of the amines of **TAQ** are important.

*2.3.1. Activity of **H2** against intracellular amastigotes*

The study on intracellular amastigotes revealed that **H2** maintains strong leishmanicidal activity. This compound is able to kill intracellular parasites inside the macrophages; therefore, it may be useful for *in vivo* treatment of the disease. Note that although the antileishmanial activity observed is for intracellular amastigotes, **H2** eliminates 97% of the parasites at 12 µM (Figure 8 B). After exposure of the infected macrophages to **H2** for 72 h, removal of this compound and reculturing the parasites in fresh media, parasite survival was observed at 3 and 6 µM, whereas concentrations of 12, 25, and 50 µM effectively killed the intracellular parasite and survival was not observed (Figure 8 C).

2.3.2. DHFR inhibition

As a second approach, the inhibition of DHFR was explored, as shown by the theoretical studies (Table 7). For experimental studies, the parasites were exposed to above LC_{50} of **H2**

(a concentration that shows an effect but does not kill all of the parasites) after they had been previously exposed to folic acid, folinic acid and ferulic acid. Folic acid competes for the active site of DHFR, as it is the natural substrate. Folinic acid does not need to undergo metabolism to contribute to DNA synthesis, and ferulic acid has an antioxidant effect. Although the effect anti-leishmanial of **H2** was decreased, differences were observed among folic acid, folinic acid and ferulic acid. The greatest inhibitor of the **H2** antileishmanial effect was folic acid, which showed a 20% increase in parasite survival compared with the control. Trimethoprim is a drug that inhibits DHFR and was used as a positive control. Parasite survival increased to 100% when the parasites were treated with folic acid before trimethoprim, demonstrating that its mechanism of action involved DHFR inhibition. An excess of folic acid was added in all cases to ensure reversibility of DHFR inhibition from the tested compounds. This complete reversibility of the antileishmanial effect with trimethoprim was not observed in the case of **H2**, in which parasite survival only reached 20% (Table 7). Therefore, we assumed that the mechanism of action of the antileishmanial effect of **H2** partially occurs via DHFR, but other mechanisms, such as a redox mechanism, could be occurring simultaneously as result of the presence of ferrocene in the molecule.

When the activity of **H2A** (acetylated **H2**) was evaluated in the docking study, improved biological activity compared to **H2** was expected due to its better affinity for the DHFR and PTR receptors. However, the results were not consistent with this hypothesis. This inconsistency can be explained by the alternate mechanism of the antileishmanial effect of **H2** and its derivatives, which is a redox mechanism resulting from ferrocene, that endows the molecule with remarkable performance against *Leishmania*, as demonstrated by its

good biological activity. The compounds **TAQ** and **4** (**TAQ** acetylated) behaved in accord with the theoretical docking prediction.

*2.3.3. Effect of **H2** on oxygen consumption by the parasite*

When the parasite is exposed to **H2**, it quickly becomes quiescent, it loses its activity as their shape wraps around, and it is finally lysed. The inhibition of parasite replication due to DHFR or PTR should take several hours to affect the parasite, but instead, the parasite dies in the presence of **H2** as soon as 20 min after it is added; thus, an alternative mechanism must be occurring. Because of this result, we investigated the inhibition of oxygen consumption, which could indicate whether the compound is able to modify the mitochondrial activity of the parasite. Thus, promastigotes of *Leishmania* parasites were treated with different concentrations of **H2** during 1 and 2 hours. If the viability of the parasite is immediately affected, then a decrease in oxygen consumption will be detected by the increase in fluorescence. The **H2** treatment reduced the fluorescence score to a level similar to that of PBS without the *Leishmania* controls, indicating that this drug somehow affects the mitochondria, the organelles that consume oxygen (Figure 9). Whether this effect is due to the respiratory chain remains to be determined.

Dithionite was used as a positive control for the abolition of oxygen concentration in the medium. For a mitochondrial damage positive control, a group of parasites was treated with sodium cyanide during two hours. In the case of **H2**, the decreased oxygen consumption, fall the fluorescence. In the case of treatment with cyanide, a similar effect was observed (Table 8).

Effect of **H2** on the *Leishmania* mitochondria. Mitotracker green is a fluorochrome that joins the mitochondria independent of their potential. Mitochondria are stained at nanomolar concentrations of Mitotracker Green FM®. Fluorescence results from the

accumulation of lipids in the mitochondria and indicates if the cells have active mitochondria. If no fluorescence is observed, the mitochondria and cells are not viable, i.e., the cells are undergoing cell death.

Propidium iodide is a fluorescent molecule that intercalates between DNA and RNA bases and is commonly used in quantitative tests of DNA content. Propidium iodide cannot permeate the cell membrane of healthy cells.

L. mexicana promastigotes that were untreated showed intense green fluorescence, as expected, and practically no parasite red stain was observed, indicating that the cells were viable and the mitochondria were fully functional.

When the promastigotes were subjected to different concentrations of the **H2**, the intense Mitotracker green FM fluorescence was not observed as the **H2** concentration increased, and the propidium iodide fluorescence was observed, indicating parasite death (Figure 10).

*2.3.4. Cytotoxic effect of **H2** on eukaryotic cells*

The cytotoxicity of **H2** was analyzed and compared with others antiparasitic compounds (nifurtimox and pyrimethamine). At a concentration of 100 μM, **H2** was slightly cytotoxic compared with the solution without the compound (Figure 11). The cytotoxicity observed in the vehicle solution should be due to DMSO. The tested concentration (100 μM) is higher than the IC_{50} against *L. mexicana.* Furthermore, evaluations were conducted to determine the influence of compounds on the metabolic activation of cells. In Figure 12, it can be seen that the pyrimethamine not affect the metabolic activity of cells, similar to control. Compound **H2** had an activity of 82%, slightly more toxic than pyrimethamine. Moreover, cells exposed to nifurtimox presented a 42% metabolic activity, indicating toxicity of this compound.

The cytotoxicity was also evaluated in macrophages, using the Alamar Blue indicator. In this evaluation the cells remained viable after 24 h at all concentrations compared to the control. This reinforces the hypothesis that the compound **H2**, is not cytotoxic (Figure 12). These results hold the interest to continue studying the compound **H2** as anti-protozoan.

Electrochemical studies

Electrochemical studies were carried out to evaluate the importance of the redox process on the biological activity, particularly with compounds containing the ferrocene moiety. We found that the half-wave potential of ferrocene not changed in the molecules.

It is important mentioning that of all of the compounds, **H2** is oxidized most easily. **H2** has an oxidation potential of -0.086 V (IA), and the magnitude of the current intensity observed in this process is three times higher than those of **TAQ** and the other compounds. That could be very important for the biological activity (Figure 13). We propose that the nitrogen in position 1 of quinazoline nucleus is oxidized because this is the location of the highest electron density (Figure 14).

The presence of the ferrocene group is important for the biological activity, which is demonstrated by the parasite growth inhibition caused by ferrocene and **FBC**. However, for ferrocene derivatives, the oxidation potential of the Fc/Fc^{+} couple does not substantially change (Table 9); therefore, the difference in activity between them results from the modification of the quinazoline nucleus.

3. Conclusions

Leishmaniasis has become a health issue due to its high incidence, especially in underdeveloped countries. There is an urgent need to develop molecules that can better treat the disease because existing molecules have become inefficient. In this study, we have two new antileishmanial agents (**H2** and **H4**). The first presented the most pronounced

potency and activity against promastigotes and amastigotes stages of parasite. The results demonstrated that leishmanicidal activity of **H2** is due to multiple mechanisms of action, which are the most significant advantage of this molecule, because they could reduce the likelihood of the parasite developing resistance. It is interesting to note that this antiparasitic effect is largely due to the presence of the ferrocene group. This moiety affords distinct characteristics to the molecule, primarily as result of the readily oxidized iron atom. Previous studies have shown that the ferrocene group can produce ROS, principally hydroxyl radicals, to exert its effect. Additionally, the quinazoline-2,4-diamine scaffold is required for biological activity, as demonstrated by the poor biological activities of **HO2**, **HO4**, **H2A** and **FBC**. In this sense, the exocyclic amino groups must be retained because they are to contribute to receptor interaction. It is worth mentioning that **H2** is electrochemically oxidized more easily with respect other quinazoline derivatives, indicating that the mechanism of action involves a type of redox reaction. Regarding the inhibition of DHFR or PTR is still involved, but it is not the primary mechanism of action of this compound because the consequences of their enzymatic inhibition would require several hours for their display; **H2** initiates its biological action from the first hour after being applied to parasites.

Other possibility is that the mitochondria are actively affected during the action of **H2**. The decrease in oxygen consumption (similar to that observed with cyanide) clearly indicates the relationship of the mechanism to inhibition of the respiratory chain, which results in apoptosis of the parasite. However, more studies are required to identify the extent of this influence on mitochondrial function. Furthermore, the fact that the promastigotes become permeable to propidium iodide is an indicator of the cell membrane damage caused by **H2**.

We are currently clarifying these hypotheses. A feature last, in cytotoxicity studies, **H2** did not showed severe toxicity in eukaryotic cells.

In regard to **H4**, which also presented an interesting activity, we could indicate that likely it has a good interaction with its receptor owing to the substituent lipoid that constitutes. Its mechanism of action may be different from **H2** because it does not present in its structure the ferrocene entity, and its antiparasitic effect is manifested after 24 h of exposure. We will focus on studying in greater detail the mechanism of activity and optimization of this compounds in the future.

Finally, we emphasize that there are new opportunities to develop novel drugs that are more active against intracellular parasites, such as Leishmania, and that present only low toxicity to the host. The results presented in this study advance the fight against orphan parasitic diseases, which often cause death.

4. Experimental section

3.1.*Chemistry*

Melting points were determined in open capillary tubes with a Büchi B-540 melting point apparatus and are uncorrected. Reactions were monitored by TLC on 0.2 mm precoated silica gel 60 F254 plates (E. Merck) and were visualized by irradiation with a UV lamp. Silica gel 60 (70–230 mesh) was used for column chromatography. IR spectra were recorded with a FT Perkin Elmer 16 PC spectrometer on KBr disks. ^{1}H NMR spectra were measured with a Varian EM-390 (300 MHz) spectrometer. Chemical shifts are given in ppm relative to tetramethylsilane (Me_4Si, δ = 0), and J values are given in Hz. Splitting patterns have been designated as follows: s, singlet; d, doublet; q, quartet; dd, doublet of doublet; t, triplet; m, multiplet; br. s, broad singlet. MS data were recorded on a JEOL JMS-SX102A spectrometer by FAB [(FAB(+)]. Elemental analyses (C, H, N) for the new

compounds were performed on a Fisons EA 1108 instrument and were within ±0.4% of the theoretical values of the proposed structures. The catalytic hydrogenation reactions were carried out in a Parr shaker hydrogenation apparatus. The starting materials 5-nitroanthranilonitrile, guanidine hydrochloride, and aniline are commercially available (Sigma Aldrich).

The percent purity for compounds **H1**, **H2**, **H3**, **H4**, **H5**, **H2A**, **HO2**, **HO4** and **FBC** was calculated by chromatographic analysis. Standard solutions of all of the compounds were dissolved in methanol grade HPLC, and the volume of injection was 20 µL. The methanol and acetonitrile used for the mobile phase were of chromatographic grade (J.T. Baker, Phillipsburg, NJ, U.S.A). Water was deionized and osmosed using a Milli-Q® system (Millipore, Bedford, MA, U.S.A). The phosphates were of analytical grade. The HPLC system consisted of a Waters Alliance e2695 separation module autosampler and a 2489 dual λ absorbance UV/Visible detector coupled with EmpowerTM software (Waters, Milford, MA, U.S.A). The analytical column was an Acentis® RP-Amide column (150 mm x 4.6 mm ID, particle size 5 µm) (Supelco, Sigma-Aldrich, U.S.A) protected by a compatible guard column. The mobile phase consisted of 10 mM phosphate buffer at pH 3.3 and acetonitrile (60:40 v/v). The assay run time was 8 min with a flow rate of 1.00 mL/min, and it was carried out at 30 °C. Absorbance was measured at 240 and 272 nm.

*4.1.1. 5,6-dicloro-1-(2,2-dietoxiethyl)-2-(trifluoromethyl)-1H-benzimidazole (**1**)*

Compound **G2** (1.43 g, 3.8 mmol) was reacted with 2-bromo-1,1-diethoxyethane (5.7 mol) and sodium carbonate (1.19 g, 11.23 mmol) in *N*,*N*-dimethylformamide (1 mL) at 110 °C for 10 h. Then, the reaction mixture was poured in cold water, and the solid was filtered and dried. Recrystallization of the powder from CH_2Cl_2 yielded cream-colored crystals (**1**)

(1.93 g, 92%, Mp: 76.8–77.6 °C), TLC (hexane/$CHCl_3$/ethyl acetate = 50/35/15) R_f = 0.65. IR (KBr): 3437 (C-H), 1133 (C-O), 1121 (C-F), 1078 (C-Cl). ^{1}H NMR (DMSO-d_6): 1.09 (t, J = 7, 6H, CH_3), 3.41 (m, J_1 = 9, J_2 = 7, 2H, OCH_2), 3.74 (m, J_1 = 9, J_2 = 7, 2H, OCH_2), 4.33 (d, J = 5, 2H, NCH_2), 4.66 (t, J = 5, 1H, OCHO), 7.79 (s, 1H, CH, aromatic), 7.89 (s, 1H, CH, aromatic); ^{13}C NMR (DMSO-d_6): 15.20, 48.77, 64.65, 101.72, 114.27, 120.20, 122.34, 128.21, 129.79, 135.53, 140.11, 142.09. Anal. Calcd for $C_{12}H_{13}N_5O_2$: C, 46.61; H, 2.93; N, 27.18. MS (+FAB) m/z = 371 (M+1).

*4.1.2. [5,6-dichloro-2-(trifluoromethyl)-1H-benzimidazole-1-yl]acetaldehyde (**2**)*

Compound **1** (1 g, 2.7 mmol) was dissolved en CH_2Cl_2 (4 mL) and reacted with a solution 1 M of BBr_3 in CH_2Cl_2 (10.77 mL, 10.77 mmol). Then, the reaction mixture was transferred into cold water, and the solution was extracted with ethyl acetate (three portions of 50 mL). The organic layer was concentrated and yielded a dark oil, which was immediately used in the next reaction (1.93 g, 99%) (TLC, hexane/$CHCl_3$/ethyl acetate = 50/35/15; R_f = 0.51).

*4.1.3. 6-nitroquinazoline-2,4-diamine (**3**)*

Sodium hydroxide (3.4 g, 85 mmol) was added to a solution of guanidine hydrochloride (3.65 g, 38 mmol) in ethanol, and the reaction was stirred for 20 min at room temperature. The solution was then stirred under reflux for 6 h with 5-nitroanthranilonitrile (5 g, 31 mmol) in 1-propanol (40 mL). Then, the reaction mixture was cooled to 0 ^{0}C. The solid was filtered off, washed with cold water, washed with cold ethanol and dried. An orange solid product was obtained (5.4 g, 86%, Mp: 360 °C), TLC (2-butanol/acetic acid/water = 80/20/5) R_f = 0.4. IR (KBr): 3464 and 3440 (N-H), 1614 (C-H, aromatic), 1325 (NO_2). ^{1}H NMR (DMSO-d_6): 6.77 (s, 2H, NH_2), 7.22 (d, J = 9, 1H, aromatic), 7.86 (s, 2H, NH_2), 8.21 (dd, J_1 = 3, J_2 = 9, 1H, aromatic), 9.08 (d, J = 3, 1H, aromatic); ^{13}C NMR (DMSO-d_6):

108.84, 121.92, 124.87, 126.63, 139.12, 157.28, 163.00, 163.025. Anal. Calcd for $C_{12}H_{13}N_5O_2$: C, 46.83; H, 3.44; N, 34.13.

*4.1.4. N-[2-(acetylamino)-6-aminoquinazolin-4-yl]acetamide (**4**)*

Compound **3** (1 g, 4.87 mmol) and acetic anhydride (1 mL) were heated at 100 ^{o}C for 12 h. Then, the reaction mixture was poured into cold water, and the solid was filtered off, washed with cold water at pH 7 and dried. A yellow solid (**3a**) was obtained (0.89 g, 65%, Mp: 278 °C), TLC ($CHCl_3$/MeOH = 60/40) R_f = 0.8. Anal. Calcd for $C_{12}H_{11}N_5O_4$: C, 49.83; H, 3.83; N, 24.21. Found: C, 49.99; H, 3.11; N, 23.81.

The catalytic reduction of **3a** (0.5 g, 1.73 mmol) with hydrogen and Pd/C (10%) (0.05 g) was carried out on a Parr assembly at 60 psi at room temperature for 1 h. The catalyst was then removed by filtration, and the filtrate was concentrated on a rotavapor under reduced pressure to yield **4** (0.34 g, 76%, Mp = 238 °C), TLC ($CHCl_3$/MeOH = 60/40) R_f = 0.67. IR (KBr): 3353 and 3230 (N-H). ^{1}H NMR (DMSO-d_6): 2.2 (s, *3*H, CH_3), 2.34 (s, 3H, CH_3), 5.61 (br. s, 2H, NH_2), 7.04 (d, J = 3, 1H, aromatic), 7.28 (dd, J_1 = 8, J_2 = 3, 1H, aromatic), 7.5 (d, J = 8, 1H, aromatic), 10.46 (br. s, 1H, NH amide), 10.22 (br. s, 1H, NH amide); ^{13}C NMR (DMSO-d_6): 24.51, 102.37, 116.82, 126.02, 127.48, 145.16, 146.55, 150.08, 156.08, 169.18, 170.73. Anal. Calcd for $C_{12}H_{13}N_5O_2$: C, 55.59; H, 5.05; N, 27.01. Found:C, 57.0; H, 4.52; N, 25.20.

*4.1.5. 2-amino-6-nitroquinazolin-4(3H)-one (**5**)*

Compound **3** (2 g, 9.7 mmol) was refluxed in 75 mL of HCl (6 N) for 2 weeks. The solution was then cooled and adjusted to pH 7 with a saturated solution of Na_2CO_3. The solid was filtered and washed repeatedly with water. A yellow solid was obtained (1.5 g, 75%, Mp: 351.5-352.5 °C), TLC ($CHCl_3$/MeOH = 80/20) R_f = 0.53. IR (KBr): 3572 and 3437 (N-H), 1704 (C=O), 1330 (NO_2). ^{1}H NMR (DMSO-d_6): 7.06 (br. s, 2H, NH_2), 7.28 (d, J = 9, 1H,

aromatic), 8.30 (dd, J_1 = 3, J_2 = 9, 1H, aromatic), 8.61 (d, J = 3, 1H, aromatic), 11.74 (br. s, 1H, NH); ^{13}C NMR (DMSO-d_6): 116.71, 123.13, 125.23, 127.76, 141.05, 154.87, 156.84, 162.04. Anal. Calcd for $C_{12}H_{13}N_5O_2$: C, 46.61; H, 2.93;N, 27.18. Found:C, 47.0; H, 2.71; N, 28.12.

*4.1.6. 4-amino-6-nitroquinazolin-2(1H)-one (**6**)*

Urea and 5-nitroantranilonitrile (2 g) were heated at 160 ° C for 2 hours with agitation. The mixture was then transferred into cold water. The solid was filtered and washed repeatedly with water. A yellow compound was obtained (0.34 g, 77%, Mp: 351.7- 354.4 °C), TLC ($CHCl_3$/MeOH = 80/20) R_f = 0.82. IR (KBr): 3444 and 3333 (N-H), 1703 (C=O), 1317 (NO_2). ^{1}H NMR (DMSO-d_6): 7.24 (d, J = 9, 1H, aromatic), 8.09 (br. s, 2H, NH_2), 8.37 (dd, J_1 = 2, J_2 = 9, 1H, aromatic), 9.07 (d, J = 2, 1H, aromatic), 11.29 (br. s, 1H, NHCO). ^{13}C NMR (DMSO-d_6): 108.22, 116.29, 122.19, 128.96, 131.89, 141.24, 147.67, 156.09, 163.73. Anal. Calcd for $C_{12}H_{13}N_5O_2$: C, 46.61; H, 2.93; N, 27.18. Found: C, 45.64; H, 2.74; N, 28.01.

*4.1.7. Synthesis of compounds **H1**, **H2**, **H3**, **H4** and **H5***

A solution of the appropriate aldehyde (1.6 mmol) and compound **4** (0.4144 g, 1.6 mmol) in methanol (80 mL) was stirred at 60 ºC for 2 days. Then, the reaction mixture was cooled to 0 °C, and $NaBH_4$ (0.09 g, 2.37 mmol) was added. Subsequently, the reaction mixture was stirred at room temperature for 12 h. Next, the reaction mixture was concentrated on a rotavapor apparatus under reduced pressure, and cold water was added. The solid was filtered off, washed with cold water and dried.

*4.1.8. N^6-(4-nitrobenzyl)quinazoline-2,4,6-triamine (**H1**)*

Red powder (0.41 g, 82%, Mp: 215-218 °C). TLC (2-butanol/acetic acid/water = 80/20/5) R_f = 0.54. IR (KBr): 3369 (N-H), 1517 (-NO_2); ^{1}H NMR (DMSO-d_6): 4.45 (d, J = 6, 2H,

CH_2), 5.71 (br. s, 2H, NH_2), 6.25 (t, *J* = 6, 1H, NH), 7.03 (m, 5H, NH_2, C-H quinazoline), 7.67 (d, *J* = 8, *2*H, p-nitrobenzyl), 8.21 (d, *J* = 8, *2*H, p-nitrobenzyl); ^{13}C NMR (DMSO-d_6): 46.16 (CH_2), 100.66 (CH, quinazoline), 110.93 (C, quinazoline), 123.17 (CH, quinazoline), 123.32 (CH, p-nitrobenzyl), 128.44 (CH, p-nitrobenzyl), 142.35 (C-NH, quinazoline), 144.44 (C, quinazoline), 146.36 (C, p-nitrobenzyl), 148.91 (C-NO_2), 158.18 (C-NH_2, quinazoline), 161.435 (C-NH_2, quinazoline); Anal. Calcd for $C_{15}H_{14}N_6O_2$: C, 58.06; H, 4.55; N, 27.08. Found: C, 57.0; H, 4.52; N, 25.20. HPLC purity of 99.9% (retention time = 3.841 min).

*4.1.9. N^6-(ferrocenmethyl)quinazolin-2,4,6-triamine (**H2**)*

Dark yellow powder (62%, Mp: 210.6-211 °C). TLC (2-butanol/acetic acid/water = 80/20/5) R_f = 0.53. IR (KBr): 3393 (N-H), 1613 (C-N), 823 (C-H ferrocene). ^{1}H NMR (DMSO-d_6): 3.98 (t, *J* = 6, 2H, CH_2), 4.12 (s, 2H, ferrocene), 4.20 (s, 5H, ferrocene), 4.32 (s, 2H, ferrocene), 5.68 (t, *J* = 6, 2H, NH_2), 6.23 (s, 2H, NH_2), 7.03 (m, 3H, aromatic quinazoline), 11.24 (br. s, 1H, NH). ^{13}C NMR (DMSO-d_6): 43.01 (CH_2), 67.33 (CH, ferrocene), 68.40 (CH, ferrocene), 86.10 (C, ferrocene), 100.25 (CH, quinazoline), 110.73 (C, quinazoline), 123.52 (CH, quinazoline), 124.99 (CH, quinazoline), 142.84 (C-NH, quinazoline), 145.11 (C-NH, quinazoline), 158.34 (C-NH_2, quinazoline), 161.48 (C-NH_2, quinazoline). Anal. Calcd for $C_{19}H_{19}FeN_5$: C, 61.14; H, 5.13; N, 18.76. Found: C, 61.14; H, 4.92; N, 18.03. HPLC purity of 99.9% (retention time = 3.947 min). The X-ray structure was determined.

*4.1.10. N^6-{2-[5,6-dichloro-2-(trifluoromethyl)-1H-benzimidazol-1-yl]ethyl}quinazoline-2,4,6-triamine (**H3**)*

Brown powder (0.62 g, 85%, Mp: 133-136 °C), TLC (2-butanol/acetic acid/water = 80/20/5) R_f = 0.59. IR (KBr): 3350 (N-H), 1273 (C-N), 742 (C-F); ^{1}H NMR (DMSO-d_6):

3.53 (br. s, *2*H, CH_2), 4.55 (br. s, 2H, CH_2), 5.61 (s, 1H, NH), 5.65 (s, 2H, NH_2). 6.84 (s, 1H, quinazoline), 7.07 (m, 4H, NH_2, CH quinazoline), 7.92 (br. s, 1H, benzimidazole), 8.13 (s, 1H, benzimidazole); ^{13}C NMR (DMSO-d_6): 42.89 (CH_2), 44.21 (CH_2), 100.21 (CH, quinazoline), 110.67 (C, quinazoline), 114.29 (CH, benzimidazole), 117.29 (C, benzimidazole), 121.91 (C-H, benzimidazole), 123.27 (CH, quinazoline), 124.89 (CH, quinazoline), 126.31 (C-Cl, benzimidazole), 127.88 (C-Cl, benzimidazole), 135.31 (C, benzimidazole), 139.76 (C-CF_3), 140.00 (CF_3), 141.80 (C-NH, quinazoline), 144.45 (C, quinazoline), 156.66 (C-NH_2, quinazoline), 161.98 (C-NH_2, quinazoline). MS (+FAB) m/z = 456 (M+1); HRMS (+FAB) calcd for $C_{18}H_{15}Cl_2F_3N_7$: 456.07. Found: 456.07. HPLC purity of 99.9% (retention time = 3.188 min).

*4.1.11. N^6-(4-methoxybenzyl)quinazoline-2,4,6-triamine (**H4**)*

Yellow powder (0.19 g, 40%, Mp: 204.1-205.2 °C). TLC ($CHCl_3$/MeOH = 80/20) R_f = 0.73. IR (KBr): 3450 and 3328 (N-H), 1639 (C-N), 1469 and 1563 (C=C Ar), 1243 (C-O-C); ^{1}H NMR (DMSO-d_6) ppm: 3.72 (s, 3H, CH_3), 4.20 (d., J = 6, 2H, CH_2), 5.53 (br. s, 2H, NH_2), 5.81 (t, J = 6, 1H, NH), 6.89 (d, J = 9, 2H, p-methoxybenzyl), 6.96 (br. s, 3H, NH_2, CH quinazoline), 7.03 (m, 2H, CH quinazoline), 7.35 (d, J = 9, 2H, p-methoxybenzyl); ^{13}C NMR (DMSO-d_6): 46.69 (CH_2), 55.45 (CH_3-O), 100.89 (CH, quinazoline), 111.15 (C, quinazoline), 114.02 (CH, p-methoxybenzyl), 123.91 (CH, quinazoline), 125.35 (CH, quinazoline), 129.42 (CH, p-methoxybenzyl), 132.31 (C, p-methoxybenzyl), 143.26 (C-NH, quinazoline), 145.37 (C, quinazoline), 158.57 (C-O, p-methoxybenzyl), 158.70 (C-NH_2, quinazoline), 161.85 (C-NH_2, quinazoline). MS (+FAB) m/z = 296 (M+1); HRMS (+FAB) calcd for $C_{16}H_{18}N_5O$: 296.15. Found: 296.15. HPLC purity of 99.9% (retention time = 3.597 min).

*4.1.12. 4-{[(2,4-diaminoquinazolin-6-yl)amino]methyl}phenol (**H5**)*

Yellow powder (0.36 g, 79%, Mp: 192.1-193.7 °C). TLC ($CHCl_3$/MeOH = 70/30) R_f = 0.65. IR (KBr): 3355 (OH), 3206 (NH), 1626 (CN), 1466 and 1568 (C=C Ar); ^{1}H NMR (DMSO-d_6): 4.14 (d, J = 3, 2H, CH_2), 5.51 (br. s, 2H, NH_2), 5.70 (t, J = 3, 1H, NH), 6.73 (d, J = 8, 2H, p-hydroxybenzyl), 6.96 (br. s, 3H, NH_2, CH quinazoline), 7.03 (m, 2H, quinazoline), 7.22 (d, J = 8, 2H, p-hydroxybenzyl), 9.23 (br. s, 1H, OH); ^{13}C NMR (DMSO-d_6): 47.01 (CH_2), 101.79 (CH, quinazoline), 110.78 (C, quinazoline), 115.45 (CH, p-hydroxybenzyl), 124.31 (CH, quinazoline), 126.11 (CH, quinazoline), 129.48 (CH, p-hydroxybenzyl), 130.10 (C, p-hydroxybenzyl), 144.21 (C-NH, quinazoline), 156.79 (C-O, p-hydroxybenzyl), 159.71 (C-NH_2), 162.49 (C-NH_2, quinazoline); MS (+FAB) m/z = 282 (M+1); HRMS (+FAB) calcd for $C_{15}H_{16}N_5O$: 282.13. Found: 282.13. HPLC purity of 92 % (retention time = 3.081 min).

*4.1.13. N-{2-(acetylamino)-6-[(ferrocenmethyl)amin]quinazolin-4-yl}acetamide (**H2A**)*

A solution of ferrocencarboxaldehyde (0.5317 g, 2.48 mmol), compound **4** (0.5850 g, 2.25 mmol), and acetic acid (one drop) in *N*,*N*-dimethylformamide (1 mL) was stirred at 85 ºC for 1 h. Then, the reaction mixture was cooled to 0 °C, and $NaBH_4$ (0.09 g, 2.43 mmol) was added. Subsequently, the reaction mixture was stirred at room temperature for 12 h. Then, the reaction mixture was concentrated on a rotavapor apparatus under reduced pressure, and cold water was added. The solid was filtered off, washed with cold water and dried. Yellow powder (0.495 g, 48%, Mp: 218.3-220.9 °C). TLC ($CHCl_3$/MeOH = 80/20) R_f = 0.76. IR (KBr): 3369 and 3244 (N-H), 1693 y 1668 (C=O), 825 (C-H ferroceno). ^{1}H NMR (DMSO-d_6): 2.2 (s, 3H, CH_3), 2.49 (s, 3H, CH_3), 4.1 (d, J = 6, 2H, CH_2), 4.13 (t, J = 2, 2H, ferrocene), 4.22 (s, *5*H, ferrocene), 4.34 (t, J = 2, 2H, ferrocene), 6.17 (t, J = 6, 1H, NH), 7.10 (d, J = 2, 1H, quinazoline), 7.4 (dd, J = 9, J = 2.4, 1H, quinazoline), 7.47 (d, J = 9, 1H, quinazoline), 10.52 (br. s, 1H, NH amide), 10.2 (br. s, 1H, NH amide). ^{13}C NMR (DMSO-

d_6): 24.38 and 25.31 (CH_3,amide), 42.40 (CH_2), 67.43 (CH, ferrocene), 68.43 (CH, ferrocene), 85.55 (C, ferrocene), 97.99 (CH, quinazoline), 115.45 (C, quinazoline), 125.86 (CH, quinazoline), 127.13 (CH, quinazoline), 145.11 (C-NH, quinazoline), 146.13 (C, quinazoline), 149.87 (C-amide, quinazoline), 155.58 (C-NHCO, quinazoline), 169 (C=O, amide), 171.75 (C=O, amide). EM-[FAB(+)] m/z=457. HRMS (+FAB) calcd for $C_{23}H_{24}FeN_5O_2$: 457.1196. Found: 457.1170. HPLC purity of 99.9% (retention time = 3.435 min).

*4.1.14. 2-amino-6-[(4-ferrocenylmethyl)amino]quinazolin-4(3H)-one (**HO4**)*

The catalytic reduction of **4** (1 g, 4.85 mmol) with hydrogen and Pd/C (10%) (0.1 g) was performed on a Parr assembly at 60 psi at room temperature for 1 h. The catalyst was filtered off, and the filtrate was concentrated on a rotavapor apparatus under reduced pressure. A light brown compound (0.6 g) was obtained (**4a,** yield= 70%), and it rapidly darkened; therefore, it was used immediately. A solution of ferrocencarboxaldehyde (0.21 g, 0.9813 mmol) and the compound obtained from the above reduction (**4a**) (0.15 g, 0.8514 mmol) in methanol (80 mL) was stirred at 60 ºC for 2 days. Then, the reaction mixture was cooled to 0 ºC, and $NaBH_4$ (0.064 g, 1.69 mmol) was added. Subsequently, the reaction mixture was stirred at room temperature for 12 h. Then, the reaction mixture was concentrated on a rotavapor apparatus under reduced pressure, and cold water was added. The solid was filtered off, washed with cold water and dried. Brown powder (0.030 g, 10%, Mp: 171.2-173.1),TLC ($CHCl_3$/MeOH = 80/20) R_f = 0.6. IR (KBr): 3410 (N-H), 1644 (C=O), 825 (C-H ferrocene). ^{1}H NMR (DMSO-d_6): 3.99 (d, J = 6, 2H, CH_2), 4.12 (br. s, 2H, ferrocene), 4.18 (s, 5H, ferrocene), 4.26 (br. s., 2H, ferrocene), 5.64 (t, J = 6, 1H, NH), 5.9 (br. s, 2H, NH_2), 7.02 (m, 3H, CH quinazoline), 10.78 (br. s, 1H, NHCO). ^{13}C NMR (DMSO-d_6): 42.77 (CH_2), 67.26 (CH, ferrocene), 68.26 (CH, ferrocene), 68.14 (CH,

ferrocene), 86.28 (C, ferrocene), 104.28 (CH, quinazoline), 117.62 (CH, quinazoline), 122.33 (CH, quinazoline), 133.40 (C, quinazoline), 143.99 (C, quinazoline), 151.62 (C-NH_2), 166.48 (C=O). EM-[FAB(+)] m/z=375. HRMS (+FAB) calcd for $C_{19}H_{19}FeN_4O$: 375.0903. Found: 375.0865. HPLC purity of 98 % (retention time = 4.364 min).

*4.1.15. 4-amino-6-[(4-ferrocenylmethyl)amino]quinazolin-2(1H)-one (**HO2**)*

The catalytic reduction of **5** (1 g, 4.85 mmol) with hydrogen and Pd/C (10%) (0.1 g) was performed on a Parr assembly at 60 psi at room temperature for 1 h. The catalyst was then filtered, and the filtrate was concentrated on a rotavapor apparatus under reduced pressure. A light brown compound (0.3 g) was obtained (**5a**, 35%), and it rapidly darkened; therefore, it was used immediately. A solution of the appropriate aldehyde (0.21 g, 0.9813 mmol) and the compound obtained from the above reduction (**5a**) (0.15 g, 0.8514 mmol) in methanol (80 mL) was stirred at 60 ºC for 2 days. Then, the reaction mixture was cooled to 0 °C, and $NaBH_4$ (0.09 g, 1.5 eq.) was added. Subsequently, the reaction mixture was stirred at room temperature for 12 h. Then, the reaction mixture was concentrated on a rotavapor apparatus under reduced pressure, and cold water was added. The solid was filtered off, washed with cold water and dried. Brown powder (0.040 g, 13%, Mp: 186.3-187.7 °C), TLC ($CHCl_3$/MeOH = 80/20) R_f = 0.27. IR (KBr): 3366 and 3366 (N-H), 1628 (C=O), 826 (C-H ferrocene). ^{1}H NMR (DMSO-d_6): 3.97 (d, J = 5, 2H, CH_2), 4.13 (br. s, 2H, ferrocene), 4.23 (s, 5H, ferrocene), 4.34 (br. s, 2H, ferrocene), 5.47 (t, J = 5, 1H, NH), 6.94 (d, J = 7, 1H, CH, quinazoline), 7.01 (d, J = 7, 1H, CH, quinazoline), 7.07 (s, 1H, CH, quinazoline), 7.73 (br. s, 2H, NH_2), 10.44 (br. s, 1H, NHCO). ^{13}C NMR (DMSO-d_6): 43.28 (CH_2), 67.85 (CH, ferrocene), 68.88 (CH, ferrocene), 69.66 (CH, ferrocene), 86.37 (C, ferrocene), 103.02 (CH, quinazoline), 116.08 (CH, quinazoline), 123.18 (CH, quinazoline), 144.06 (C, quinazoline), 156.37 (C=O), 160.89 (C-NH_2). EM-[FAB(+)] m/z=375. HRMS

595 (+FAB) calcd for $C_{19}H_{19}FeN_4O$: 375.0903. Found: 375.0865. HPLC purity of 99.9%
596 (retention time = 3.604 min).

597 *4.1.16. N-ferrocenylmethylaniline (**FBC**)*

598 A solution of ferrocencarboxaldehyde (0.15 g, 0.7 mmol) and aniline (0.072 g, 0.77 mmol)
599 in methanol(30 mL) was stirred at 60 ºC during 2 days. Then, the reaction mixture was
600 cooled to 0 °C, and $NaBH_4$ (0.080 g, 2.11 mmol) was added. Subsequently, the reaction
601 mixture was stirred at room temperature for 12 h. Then, the reaction mixture was
602 concentrated on a rotavapor apparatus under reduced pressure, and cold water was added.
603 The solid was filtered off, washed with cold water and dried. Brown powder (0.089 g, 40%,
604 Mp: 84.9-85.3 °C). TLC (hexane/ethyl acetate = 80/20) R_f = 0.67. IR (KBr): 3369 and 3244
605 (N-H), 1693 and 1668 (C=O), 825 (C-H ferrocene). ^{1}H NMR (DMSO-d_6): 3.95 (d, J = 3,
606 2H, CH_2), 4.09 (br. s, 2H, ferrocene), 4.18 (s, 5H, ferrocene), 4.26 (br. s, 2H, ferrocene),
607 5.60 (br. s, 1H, NH), 6.51 (t, J = 6, 1H, aromatic), 6.64 (d, J = 9, 2H, aromatic), 7.47 (t, J =
608 6, 2H, aromatic). ^{13}C NMR (DMSO-d_6): 42.23 (CH_2), 67.24 (CH, ferrocene), 68.40 (CH,
609 ferrocene), 86.47 (C, ferrocene), 112.12 (CH, meta-aniline), 115.59 (CH, para-aniline),
610 128.77 (ortho-aniline), 148.68 (C-NH, aniline). EM-[FAB(+)] m/z=291. HRMS (+FAB)
611 calcd for $C_{17}H_{18}FeN$: 291.0705. Found: 291.0690.

612 *4.2. X-ray crystallographic*

613 The **H2** crystal obtained from ethanol was mounted on a glass fiber and was studied with an
614 Oxford Diffraction Gemini "A" diffractometer with a CCD area detector ($\lambda_{MoK\alpha}$ = 0.71073
615 Å, monochromator: graphite) source equipped with a sealed tube X-ray source at 130 K.
616 The unit cell constants were determined with a set of 15/3 narrow frame/run (1° in ω)
617 scans. A data set consisted of 303 frames of intensity data collected with a frame width of

1° in ω, a counting time of 25 s/frame, and a crystal-to-detector distance of 55.00 mm. The double pass method of scanning was used to exclude any noise. The collected frames were integrated using an orientation matrix determined from the narrow frame scans. The CrysAlisPro and CrysAlis RED software packages were used for data collection and data integration [25]. Analysis of the integrated data did not show any decay. The final cell constants were determined by a global refinement of 6196 reflections ($\theta < 26.06$ °). The collected data were corrected for absorbance using an analytical numerical absorption correction, which employs a multifaceted crystal model based on expressions of the Laue symmetry using equivalent reflections [26]. Structure solution and refinement were performed with the following programs: the SHELXL97 program for molecular graphics, the ORTEP-3 program for Windows and the WinGX software for the preparation of materials for publication [27,28,29].

The full-matrix least-squares refinement was conducted by minimizing $(Fo^2 - Fc^2)^2$. All of the non-hydrogen atoms were refined anisotropically. The H atoms of the methanol solvent (H-O) and the amine group (H-N) were located in a difference map and refined isotropically with a U_{iso}(H) value of 1.5 and 1.2 U_{eq} for (O) and (N), respectively. The H atoms attached to C atoms were placed in geometrically idealized positions and refined as riding on their parent atoms, with C—H = 0.95 – 0.99 Å with U_{iso} (H) = 1.2U_{eq}(C) for methylene and aromatic groups, and U_{iso} (H) = 1.5 U_{eq}(C) for the methyl group. The crystal data and experimental details of the structure determinations are listed in Table 5.

4.3. Modeling studies

To construct DHFR *Leishmania major*, the *Trypanosoma cruzi* enzyme (ID-PDB: 2H2Q Key) was used as the template. First, the amino acids were corrected with the Modeler

641 program [30]. Classical MD simulations were performed using the NAMD2.6 program
642 using the CHARMM27 force field, and water molecules were added using the VMD
643 program [31,32]. The structure was neutralized with 4 sodium ions after being immersed in
644 a TIP3P water box containing 9249 water molecules. The equilibration protocol began with
645 1500 minimization steps followed by 30 ps of MD at 310 K with fixed protein atoms. Then,
646 the entire system was minimized for 1500 steps (at 0 K) and then heated gradually from 10
647 to 310 K by temperature reassignment during the first 60 ps of 100 ps equilibration
648 dynamics without restraints. The final step was a 30 ps NTP dynamics using the Nose-
649 Hoover Langevin piston pressure control 28 at 310 K and 1.01325 bar for density (volume)
650 fitting. From this point, the simulation was continued in the NTV ensemble during 5 ns.
651 The periodic boundary conditions and the particle-mesh Ewald method were applied for a
652 complete electrostatics calculation. The dielectric water constant was used, and the
653 temperature was maintained at 310 K using Langevin dynamics. The structure was allowed
654 to converge, which was reached at 10 ns. A snapshot was obtained at this time for the
655 computational docking.
656 The docking was also performed for PTR from the structure for this enzyme obtained after
657 crystallization with triaminoquinazoline (ID-PDB: 1WOC), which also validated the study.
658 The program AutoDock4 was used [33]. For the docking of both proteins, the water
659 molecules were removed, and the active site was defined as all of the residues within a grid
660 of 60 Aº x 60 Aº x 60 Aº centered in the active site, with an initial population of 100
661 randomly placed individuals and a maximum number of 1.0 X 10^7energy evaluations. The
662 compounds for docking were drawn in Gauss view 3.0. Before docking, the compounds
663 were subjected to energy minimization using the hybrid functional B3LYP with a 6, 31
664 G(d,p) basis set. The crystallographic structure was taken as the starting point for

665 construction of the compounds. These constructs were minimized using the Gaussian 03
666 program. The most stable tautomers were chosen. We assumed that ferrocene has aromatic
667 character. The values of K_d and ΔG were taken from the conformation with the minimum
668 energy, and a large K_d value has been reported elsewhere. This study was validated by
669 comparing the conformation of triaminoquinazoline from the crystalline structure and the
670 docking result, which achieved a satisfactory result. The graphics were prepared with
671 OriginLab, and the figures were prepared with ACD/ChemSketch for the structures
672 (ACD/Structure Elucidator, version 12.01, Advanced Chemistry Development, Inc.,
673 Toronto, ON, Canada, www.acdlabs.com, 2013) and PyMOL for the proteins and ligands
674 (The PyMOL Molecular Graphics System, Version 1.2r3pre, Schrödinger, LLC).

675 *4.4. Biological studies*

676 *4.4.1.Antiprotozal activity*

677 The antileishmanial activity was tested in an *in vitro* culture of promastigotes the
678 *Leishmania mexicana* strain MHOM/BZ/61/M379 growing in Dulbecco's modified Eagle's
679 medium (DMEM) containing L-glutamine and glucose (4,500 mg per liter), without sodium
680 bicarbonate (GIBCO, Grand Island, NY), supplemented with 10% fetal calf serum
681 (GIBCO). The experiments were performed in 24-well plates for tissue culture by adding
682 0.5 mL of one of the serial dilutions of the compound solubilized in a specified solvent (in a
683 ratio of 1:10 of compound:media) to each well along with 0.5 mL 2x 10^6 parasites/mL. The
684 plates were stored at 26 °C for 72 h. The parasite density was counted with a
685 hemacytometer in triplicate.

686 The effect of the compounds was tested on intracellular macrophages as previously
687 described [34]. Briefly, the intracellular parasites were prepared by the addition of 10^7
688 parasites, with growth at 32 °C to a monocyte monolayer in a 24-well plate of peritoneal

689 resident macrophages harvested from BALB/c male adult mice. The culture plates were
690 incubated at 32 °C under an atmosphere of 5% CO_2 for 48 h to allow internalization of the
691 parasites by the macrophages. The cultures were washed in triplicate with prewarmed
692 sterile phosphate-buffered saline (PBS) to remove extracellular parasites, and 1 mL of
693 media containing the various concentrations of the compound was added to each well. The
694 plates were returned to 32 °C under an atmosphere of 5% CO_2 for an additional 24, 48 or
695 72 h incubation. Then, the compound was removed, and fresh medium was added.
696 Subsequently, the plates were cooled to 26 °C to promote the transformation of the living
697 parasites to the motile form and to cause their release from the macrophages. The parasites
698 were counted with a hematocytometer 24 h after compound removal.
699 The results for promastigotes and intracellular amastigotes were expressed as percentage of
700 growth inhibition relative to the control. It is also possible to calculate the percent survival
701 subtracting from 100 the percentage of growth inhibition.
702 *4.4.2. DHFR inhibition*
703 This experimental study was carried out on the *in vitro* growth assay for promastigotes. The
704 concentrations evaluated of **H2** and trimetoprim on the leishmania parasites were of 2 µM
705 and 100 µM, respectively. To test DHFR inhibition by folinic acid, ferulic acid and folic
706 acid, the compounds were incubated with 20 or 100 µM with 10^6 leishmania at the
707 logarithmic phase of growth, washed and resuspended with PBS and incubated for 1 h at
708 room temperature [35]. Then, the parasites were centrifuged, the media was eliminated, and
709 the parasites were resuspended in the culture media and distributed in a 24-well plate. **H2**,
710 or trimetoprim, were then added at the desired concentration, and the plates were incubated
711 for 48 h. The percentage of living parasites was calculated using the formula: % AP = 100 x

712 (*Tc – Tp)/Tc*, where % AP is the percentage of growth inhibition for each period, and each
713 compound concentration, *Tc*, is the number of parasites/mL in the control wells, and *Tp* is
714 the average number of moving parasites/mL.

715 *4.4.3. Measurement of oxygen consumption of the Leishmania parasites*

716 The effects of the **H2** treatment on leishmania oxygen consumption were determined using
717 a BD^{tm} Oxygen Biosensor System that incorporates an oxygen-sensitive fluorophore into
718 the wells of an automation-friendly BD Falcon microplate (BD Biosciences, Bedford, MA,
719 USA). The leishmania promastigotes were deposited on the plate with the indicated
720 concentration of **H2** or the control for 1 or 2 h, and oxygen consumption was measured in a
721 Synergy 2 Microplate Reader (Bio Tek Instruments, Inc, Winooski, VT, USA). Sodium
722 cyanide was used a positive control for mitochondrial damage, and dithionite alone was
723 considered a positive control for the abolition of oxygen content in the medium. The
724 experiments were performed in triplicate. The promastigotes of *L. mexicana* were treated
725 with different concentrations of **H2** for 1 and 2 h. Dithionite was used as a positive control
726 for the abolition of oxygen concentration in the medium; for the mitochondrial damage
727 positive control, a group of parasites were treated with sodium cyanide.

728 *4.4.4. Mitochondrial functionality of Leishmania promastigotes in the presence of **H2***

729 The mitochondrial function of the *L. mexicana* strain M379 in the presence of **H2** was
730 tested using a MitoTracker probe (Invitrogen, Eugene, OR, USA) according to the
731 manufacturer's instructions. Briefly, the parasites were washed three times with PBS -
732 0.1% glucose to prevent cell lysis due to lack of nutrients. This step maintains the parasites
733 under optimal conditions before treatment with **H2**. The parasites were counted with a
734 hematocytometer chamber and adjusted to 5 X 10^6 parasites/mL. Serial concentrations of
735 **H2** were added to each well, and after 2 h of treatment, the parasites were stained with 50

μg/mL propidium iodide and 200 nM MitoTracker® Green FM. The preparations were observed using an epifluorescence microscope. In the control without **H2**, the parasites showed high fluorescence, which indicates the functional respiratory process. The parasites without **H2**, **H2** without Leishmania, sodium cyanide with Leishmania and **H2** alone were observed for fluorescence, and no fluorescence was observed (data not shown).

4.4.5. Cytotoxicity studies.

Method 1. The agar diffusion method (USP <87> cytotoxicity test) was used to this evaluation [36]. The cell line used for testing was L929, fibroblast cell from subcutaneous, adipose and areolar mouse tissues. The L929 cells were derived from ATCC catalog number CCL-1. Cells were grown in MEM medium supplemented with 10% FBS and incubated at 37 °C under 5% CO_2, as shown in the data sheet ATCC, and until a monolayer, with greater 80%, confluence, was obtained. The agar layer was tin enough to permit diffusion of test compound solution. Then compounds were placed on the agar surface on the cells. Cells cultures were incubate for 24 h at 37 °C. Each culture was examined under microscopic. Positive control was USP High density polyethylene RS. After 48 hours incubation proceeded to remove the test compound and the agar layer with the purpose of determining the metabolic ability of cells. This capacity was quantified by the metabolic dye Alamar Blue ®. The cells were incubated for 6 hours with this dye at 37 ° C and 5% CO_2 and were then quantified in a plate reader by measuring fluorescence emission of 535 nm and excitation of 595 nm. All evaluations were in triplicate.

Method 2. **H2** toxicity on peritoneal macrophages from BALB/c mice. Peritoneal macrophages were obtained from healthy BALB/c mice, washed twice with PBS, suspended in DMEM at 105/mL, dispensed in 96 wells plate at volume of 100 μL. **H2**,

759 solvent, or meglumine antimoniate were added to the wells, as was previously described for
760 efficacy experiment. Macrophages were incubated by 24 h with the test compounds and
761 then washed. Fresh media was used for additional 48 h. Alamar blue was added to measure
762 cell viability. The change in fluorescence were measured using fluorescence
763 spectrophotometry. In this case, the reduction of the dye comes from macrophages.
764 Experiments were carried out in triplicate and repeated at least twice.

765 4.5. Solubility studies.

766 The solubility was calculated according to Lipinsky et al [37]. Compound was dissolved
767 in DMSO at a concentration of 10 μg/μL. One microlitre of this solution was added at a
768 time to a non-chloride solution containing pH 7 phosphate buffer, at room temperature. The
769 additions of solutions are spaced a minute apart. A total of 14 additions were made. This
770 correspond to solubility increments of 5 pg/mL to a top value of 65 μg/mL when the buffer
771 volume is 2.5 mL (as in a UV cuvette). If it is clear that precipitation was occurring early in
772 the addition sequence, the addition was stopped, so that we had two consecutive readings
773 after the precipitate was detected. Precipitation can be detected by an absorbance increase
774 due to light scattering by precipitated particulate material in a UV spectrophotometer. In its
775 simplest implementation, the precipitation point was calculated from a bilinear curve fit to
776 the absorbance versus concentration plot and is reported in mg/mL [37]. Experiments were
777 carried out in triplicate and repeated at least twice.

778 *4.6. Electrochemical studies*

779 Electrochemical measurements were performed on a potentiostat-galvanostat Autolab
780 model PAR263A device with a three-electrode system in a 0.1 M solution of
781 tetrabutylammonium hexafluorophosphate (Bu_4NPF_6) in DMSO as the supporting

electrolyte. A carbon glass disc (0.071 cm^2) was used as the working electrode, a Pt wire was used as the auxiliary electrode, and 0.1 M (Bu_4N)Br/AgBr(s)/Ag was used as the reference electrode. The working electrode (C) was polished with alumina to ensure the absence of residues on the surface. All of the voltammograms were initiated from the open circuit potential (E_i=0), and the scan was initiated in both the positive and negative potential directions. To report the potentials used according to the IUPAC convention, the voltammograms were obtained for approximately 10^{-3} M solutions of ferrocene (Fc) in a supporting electrolyte. For the working conditions, the electroactive domain was between -2.70 and 1.60 V/Fc^+-Fc. The halfwave potentials were estimated from $E_{1/2} = (E_{ap} + E_{cp})/2$, where E_{ap} and E_{cp} are the anodic and cathodic peak potentials, respectively.

ASSOCIATED CONTENT

Supporting information

The crystallographic data were deposited at the Cambridge Crystallographic Data Center as supplementary material number CCDC 995399. Copies of the data can be obtained free of charge on application to CCDC, 12 Union Road, Cambridge CB2 1EZ, UK. E-mail:deposit@ccdc.cam.ac.uk.

ACKNOWLEDGMENTS

This study was supported by a fellowship and infrastructure purchased with funds from PAPIIT-UNAM IN213914 and research funds from CONACYT-6248. We are grateful to Rosa Isela del Villar, Georgina Duarte, Margarita Guzmán, Nayeli López and Marisela Gutiérrez from Facultad de Química, USAI, UNAM for the determination of all of the spectra. For the theoretical studies, we are grateful to DGSCA-UNAM for allowing the use of the KanBalam supercomputer.

ABREVIATIONS USED

806 PTR1, Pteridine reductase 1; DHFR, Dyhydrofolate reductase; IC_{50}, Half inhibitory
807 concentration; TAQ, Quinazoline-2,4,6-triamine; PDB, Protein Data Bank.

808
809

REFERENCES

[1] K. T. Andrews, G. Fisher, T. S. Skinner-Adams, Drug repurposing and human parasitic protozoan diseases, Int. J. Parasitol. Drugs Drug Resist. 4 (2014) 95–111.

[2] World Health Organization. Control of the leishmaniases. WHO Technical Report Series. http://www.who.int/leishmaniasis/resources/en.

[3] T. S. Tiumana, A. O. Santos, T. Ueda-Nakamuraa, B. P. Dias Filhoa, C. V. Nakamuraa, Recent advances in leishmaniasis treatment, Int. J. Infect. Dis. 15 (2011) e525–e532.

[4] R. M. Reguera, E. Calvo-Álvarez, R. Álvarez-Velilla, R. Balaña-Fouce, Target-based vs. phenotypic screenings in Leishmania drug discovery: A marriage of convenience or a dialogue of the deaf?, Int. J. Parasitol. Drugs Drug Resist. (2014). DOI: http://dx.doi.org/10.1016/j.ijpddr.2014.05.001

[5] N. Singh, M. Kumar, R. K. Singh, Leishmaniasis: Current status of available drugs and new potential drug targets, Asian Pac. J. Trop. Med. 5 (2012) 485-497.

[6] J. Mishra, S. Singh, Miltefosine resistance in Leishmania donovani involves suppression of oxidative stress-induced programmed cell death, Exp. Parasitol. 135 (2013) 397–406.

[7] I. V. Ogungbe, W. R. Erwin, W. N. Setzer, Antileishmanial phytochemical phenolics: Molecular docking to potential protein targets, J. Mol. Graph. Model. 48 (2014) 105–117.

[8] P. Gahtori, S. K. Ghosh, P. Parida, A. Prakash, K. Gogoi, H. R. Bhat, U. P. Singh, Antimalarial evaluation and docking studies of hybrid phenylthiazolyl-1,3,5-triazine derivatives: A novel and potential antifolate lead for pf-DHFR-TS inhibition, Exp. Parasitol. 130 (2012) 292–299.

[9] I. M. Kompis, K. Islam, L. R. Then, DNA and RNA Synthesis: Antifolates. Chem. Rev. 105 (2005) 593–620.

[10] B. Nare, L. W. Hardy, S. M. Beverley, The roles of Pteridine Reductase 1 and Dihydrofolate Reductase-Thymidylate Synthase in Pteridine Metabolism in the Protozoan Parasite *Leishmania major*. J. Biol. Chem. 272 (1997) 13883–13891.

[11] H. B. Ong, N. Sienkiewicz, S. Wyllie, A. H. Fairlamb, Dissecting the Metabolic Roles of Pteridine Reductase 1 in *Trypanosoma brucei* and *Leishmania major*. J. Biol. Chem. 286 (2011) 10429–10438.

[12] K. McLuskey, F. Gibellini, P. Carvalho, M. A. Avery, W. N. Hunter, Inhibition of *Leishmania major* pteridine reductase by 2,4,6-triaminoquinazoline: structure of the NADPH ternary complex. Acta Cryst. D60 (2004) 1780–1785.

[13] J. D. Berman, M. King, N. Edwards, Antileishmanial activities of 2,4-diaminoquinazoline putative dihydrofolate reductase inhibitors. Antimicrob Agents Chemother. 33 (1989) 1860–1863.

[14] D. Dive, C. Biot, Ferrocene conjugates of Chloroquine and other Antimalarials: the Development of Ferroquine, a New Antimalarial. ChemMedChem. 3 (2008) 383–391.

[15] A. Pejović , M. S. Denić, D. Stevanović, I. Damljanović, M. Vukicević, K. Kostova, M. Tavlinova-Kirilov, P. Randjelović, N. M. Stojanović, G. A. Bogdanović, P. Blagojević, M. D'hooghe, N. S. Radulović , R. D. Vukićević, Discovery of anxiolytic 2-ferrocenyl-1,3-thiazolidin-4-ones exerting GABAA receptor interaction via the benzodiazepine-binding site, Eur. J. Med. Chem. 83 (2014) 57–73.

[16] I.S. Damljanovi_c, M.D. Vuki_cevi_c, N.S. Radulovi_c, R.M. Pali_c, E. Ellmerer, Z.R. Ratkovi_c, M.D. Joksovi_c, R.D. Vuki_cevi_c, Synthesis and antimicrobial

activity of some new pyrazole derivatives containing a ferrocene unit, Bioorg. Med. Chem. Lett. 19 (2009) 1093–1096.

[17] S. Gurvinder, K. Maninderjit,C. Mohan, Benzimidazoles: the latest information on biological activities, Int. Res. J. Pharm. 4 (2013) 82–87

[18] G. Navarrete-Vázquez, R. Cedillo, A. Hernández-Campos, L. Yépez, F. Hernández-Luis, J. Valdez, R. Morales, R. Cortés, M. Hernández, R. Castillo, Synthesis and antiparasitic activity of 2-(trifluoromethyl)-benzimidazole derivatives, Bioorg. Med. Chem. Lett. 11 (2001) 187–190

[19] F. Palomares-Alonso, H. Jung-Cook, J. Pérez-Villanueva, J.C. Piliado, S. Rodríguez-Morales, G. Palencia-Hernández, N. López-Balbiaux, A. Hernández-Campos, R. Castillo, F. Hernández-Luis, Synthesis and in vitro cysticidal activity of new benzimidazole derivatives, Eur. J. Med. Chem. 44 (2009) 1794–1800.

[20] L. Kedzierski, J. M. Curtis, M. Kaminska, J. Jodynis-Liebert, M. Murias, In vitro antileishmanial activity of resveratrol and its hydroxylated analogues against Leishmania major promastigotes and amastigotes, Parasitol. Res. 102 (2007) 91–97.

[21] J. Davoll, A.M. Johnson, H.J. Davies, O.D. Bird, J. Clarke , E.F. Elslager, 2,4-Diamino-6-{[aralkyl and (heterocyclic)methyl]amino}quinazolines, a novel class of antimetabolites of interest in drug-resistant malaria and Chagas' disease, J. Med. Chem.15 (1972) 812–826.

[22] C. E. Ballou, H. O. L. Fischer, The Synthesis of Dihydroxyacetone Phosphate. J. Am. Chem. Soc. 78 (1956) 1659–1661.

[23] J. Sun, Y. Dong, L. Cao, X. Wang, S. Wang, Y. Hu, Highly Efficient Chemoselective Deprotection of O,O-Acetals and O,O-Ketals Catalyzed by Molecular Iodine in Acetone, J. Org. Chem. 69 (2004) 8932–8934.

[24] S. E. Sen, S. L. Roach, J. K. Boggs, G. J. Ewing, J. Magrath, Ferric Chloride Hexahydrate: A Mild Hydrolytic Agent for the Deprotection of Acetals. J. Org. Chem. 62 (1997) 6684–6686.

[25] Oxford Diffraction, CrysAlis CCD, and CrysAlis RED. Abingdon, UK: Oxford Diffraction Ltd.; 2009.

[26] R. C. Clark, J. S. Reid, The analytical calculation of absorption in multifaceted crystals. Acta Crystallogr. A51 (1995) 887–897.

[27] G. M. Sheldrick, A short history of SHELX. Acta Crystallogr. A64 (2008) 112–122.

[28] L. J. Farrugia, ORTEP-3 for Windows - a version of ORTEP-III with a Graphical User Interface (GUI). Appl Crystallogr. 30 (1997) 565.

[29] L. J. Farrugia, WinGX suite for small-molecule single-crystal crystallography. Appl. Crystallogr. 32 (1999) 837–838.

[30] A. Sali, T. L. Blundell, Comparative protein modelling by satisfaction of spatial restraints. J. Mol. Biol. 234 (1993) 779–815.

[31] J. C. Phillips, R. Braun, W. Wang, J. Gumbart, E. Tajkhorshid, E. Villa, C. Chipot, R.D. Skeel, L. Kale, K. Schulten, Scalable molecular dynamics with NAMD. J. Comput. Chem. 26 (2005) 1781–1802.

[32] W. Humphrey, A. Dalke, K. Schulten, VMD - Visual Molecular Dynamics. J. Molec. Graphics, 14 (1996) 33–38.

[33] G. M. Morris, R. Huey, W. Lindstrom, M. F. Sanner, R. K. Belew, D. S. Goodsell, A. J. Olson, Autodock4 and AutoDockTools4: automated docking with selective receptor flexiblity. J. Comput. Chem. 16 (2009) 2785–91.

902 [34] H. Martinez-Rojano, J. Mancilla-Ramirez, L. Quiñonez, N. Galindo-Sevilla, Activity
903 of hydroxyurea against *Leishmania mexicana*. Antimicrob. Agents Chemother. 52
904 (2008) 3642–3647.
905 [35] L. Quiñonez-Díaz; J. Mancilla, M. Avila-García, J. Ortíz-Avalos, A. Berron, S.
906 Gonzalez, Y. Paredes, N. Galindo-Sevilla, Effect of ambient temperature on the
907 clinical manifestation of experimental diffuse cutaneous leishmaniasis in a rodent
908 model. Vector Borne Zoonotic Dis. 12 (2012) 851–860.
909 [36] US Pharmacopeia (USP29). http://www.pharmacopeia.cn/v29240/usp29nf24s0_c87.html,
910 accessed 2013-01-30
911 [37] C. A. Lipinski, F. Lombardo, B. W. Dominy, P. J. Feeney, Experimental and
912 computational approaches to estimate solubility and permeability in drug discovery
913 and development settings. Adv. Drug Deliv. Rev. 23 (1997) 3–25.

Legends

Figure 1. Interaction of **TAQ** with PTR1 (ID-PDB: 1WOC).

Figure 2. H2 derivatives

Figure 3. ORTEP diagram of **H2** with displacement ellipsoids at 50% probability level for non-H atoms.

Figure 4. The hydrogen bonds N-H•••O, N-H•••N and O-H•••O lead to an infinite three-dimensional in **H2**.

Figure 5. Stable tautomers of **HO2** and **HO4** considered for molecular modeling.

Figure 6. RMSD (a) and R-gyration (b) calculations by analyzing the stability of DHFR over time.

Figure 7. Interaction of ferrocene derivatives with DHFR (A) and PTR1 (B).

Figure 8. Effect of **H2** on the promastigotes and intracellular amastigotes.

Figure 9. *L. mexicana* treated with different concentrations of **H2**.

Figure 10. The promastigotes of *L. mexicana* exposed to **H2**.

Figure 11. Fibroblast exposed to the various compounds tested at 24 hours of exposure.

Figure 12.Inhibition of metabolic activation by compounds at 48 hours of exposure.

Figure 13. Electrochemical studies for **H2** and **TAQ** in DMSO (A) and culture medium (B).

Figure 14. Electrostatic potential mapped on the electronic density from **H2**, a level B3LYP 6-31G**.

Schemes

Scheme 1. Reagents and conditions: (a) 2-bromo-1,1-diethoxyethane, Na_2CO_3, DMF, 110 ºC, 92%; (b) i-BBr_3, CH_2Cl_2; ii-H_2O, 99%; (c) guanidine hydrochloride, NaOH, EtOH-PrOH, reflux, 86%; (d) acetic anhydride, 110 ºC, 65%; (e) H_2, 10% Pd/C, MeOH, r.t. 76%; (f) MeOH, CH_3COOH (a drop), 50 ºC, 2 days; (g) 0 ºC, $NaBH_4$, then r.t. for 24 h, 40-90%.

Scheme 2. Reagents and conditions: (a) guanidine hydrochloride, NaOH, EtOH-PrOH, reflux, 86%; (b) HCl (2 M), 90 °C, 24 h, 75%; (c) Urea, 160 °C, 77% (d) H_2, 10% Pd/C, MeOH, r.t, 30-70%; (e) MeOH, 60 ºC, 1 h; (f) 0 ºC, $NaBH_4$, then 24 h r.t. 10-15%; (g) DMF, 85 ºC, 1 h; (h) 0 ºC, $NaBH_4$, then 24 h at r.t. under N_2 atmosphere, 48%.

Tables

Table 1. Derivatives of **TAQ** with antiparasitic moieties.

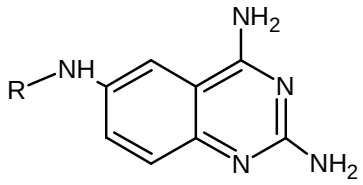

Compound	R
H1	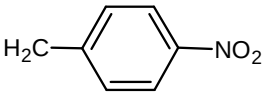
H2	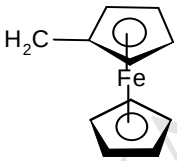
H3	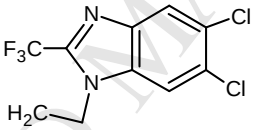
H4	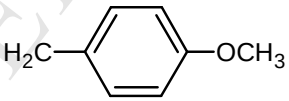
H5	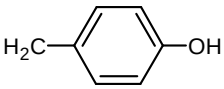

Fe(1)-C(1)	2.035(2)
Fe(1)-C(2)	2.044(2)
Fe(1)-C(3)	2.051(2)
Fe(1)-C(4)	2.042(2)
Fe(1)-C(5)	2.045(2)
N(1)-C(11)	1.402(3)
N(1)-C(19)	1.465(3)
C(1)-C(19)	1.498(3)
C(19)-N(1)-C(11)-C(12)	20.8(3)
N(1)-C(11)-C(16)-C(15)	-176.1(2)
C(18)-N(2)-C(17)-N(4)	-179.79(19)
C(14)-N(3)-C(18)-N(2)	-0.6(3)
C(14)-N(3)-C(18)-N(5)	179.9(2)
C(11)-N(1)-C(19)-C(1)	165.1(2)
C(2)-C(1)-C(19)-N(1)	-106.5(3)
C(5)-C(1)-C(19)-N(1)	70.2(3)

D-H...A	d(D-H)	d(H...A)	d(D...A)	<(DHA)
N(4)-H(4G)...N(2)#1	0.881(17)	2.073(18)	2.953(2)	178(3)
N(1)-H(1F)...O(1C)#2	0.890(18)	2.15(2)	2.984(3)	155(3)
N(5)-H(5F)...O(1A)#1	0.894(17)	2.252(19)	3.126(3)	166(3)
O(1B)-H(1E)...N(3)#3	0.827(18)	1.878(19)	2.701(2)	173(3)

Symmetry transformations used to generate equivalent atoms:
#1 -x+2,-y,-z #2 -x+1,-y,-z+1 #3 x,y+1,z

Identification code	h2-etoh
Empirical formula	C25 H37 Fe N5 O3
Formula weight	511.45
Temperature	130(2) K
Wavelength	0.71073 Å
Crystal system	Triclinic
Space group	P-1
Unit cell dimensions	a = 9.9983(3) Å
	b = 10.8761(4) Å
	c = 12.9003(5) Å
	α = 101.074(3)°.
	β = 101.357(3)°.
	γ = 103.365(3)°.
Volume	1295.92(8) $Å^3$
Z	2
Density (calculated)	1.311 Mg/m^3
Absorption coefficient	0.617 mm^{-1}
F(000)	544
Crystal size	0.2994 0.2592 0.2057 mm^3
Theta range for data collection	3.42 to 26.06°.
Index ranges	-12<=h<=9, -10<=k<=13, -15<=l<=15
Reflections collected	9490
Independent reflections	5110 [R(int) = 0.0207]
Completeness to theta = 26.06°	99.7 %
Refinement method	Full-matrix least-squares on F^2
Data / restraints / parameters	5110 / 8 / 334
Goodness-of-fit on F^2	1.069
Final R indices [I>2sigma(I)]	R1 = 0.0427, wR2 = 0.1169
R indices (all data)	R1 = 0.0528, wR2 = 0.1215
Largest diff. peak and hole	0.790 and -0.696 $e.Å^{-3}$

	DHFR		PTR	
Compound	Kd (μM)	ΔG (Kcal)	Kd (μM)	ΔG (Kcal)
H1	0.241	-9.03	1.430	-7.98
H2	0.379	-8.76	1.460	-7.96
H3	0.752	-8.35	0.093	-9.59
H4	1.580	-7.91	2.850	-7.57
H5	1.020	-8.17	2.400	-7.67
HO2 (most stable tautomer)	3.650	-7.42	1.350	-8.01
HO4 (most stable tautomer)	1.700	-7.87	0.223	-9.08
H2A	0.087	-9.63	0.008	-13.45
TAQ	83.98	-5.56	58.75	-5.77
3	15.81	-6.55	0.2615	-8.98

Compound	% inhibition growth of parasite (100 µM)(±SD)	IC_{50} (µM)	Solubility (mg/mL) Phosphate buffer pH=7.4
Control	0	ND	ND
H1	20 ± 3.3	>100	0.13 ± 0.05
H2	100	0.93 ± 0.1	0.63 ± 0.03
H3	0	ND	0.51 ± 0.08
H4	100	14.59 ± 1.3	0.25 ± 0.05
H5	0	ND	0.38 ± 0.01
HO2	60 ± 3.2	93.1 ± 2.5	0.15 ± 0.08
HO4	44 ± 2.8	>100	0.06 ± 0.06
H2A	24 ± 5.2	>100	1.51 ± 0.02
FBC	70 ± 1.4	ND	0.10 ± 0.05
Ferrocene	73 ± 2.7	ND	0.03 ± 0.01
TAQ	0	ND	> 9.00
Glucantime	100	182.7 ± 0.19	ND
Trimetoprim	30 ± 3.8	>100	ND
Pyrimethamine	50 ± 1.9	100 ± 1.9	ND

ND: not determinated

Treatment	% Oxigen consumption
Leishmania	100
PBS	20.4%± 1.2
L. mexicana treated with sodium cyanide (0.02 μM)	20.5%± 1
L. mexicana treated with **H2** (100 μM)	22.5%± 1
Sodium dithionite (5.74 mM)	175.9%± 5.8

	N-Oxidation	Ferrocene[1]		*N*-Oxidation		
	DMSO	DMSO	Culture medium	DMSO		Culture medium
Compound	IA		IB	II	III	II
		($E_{1/2Ferr/Ferr+}$)				
H2	-0.086	0.037	0.134	0.21	0.681	0.31
HO2		0.020	0.105		0.46	0.21
HO4		0.021	0.126	0.267	0.86	0.39
H2A		0.047	0.127		0.619	0.33
TAQ	-0.026				0.668	0.383
3					0.665	0.652
FBC		0.011	0.136		0.614	0.68

Electrochemical studies in DMSO and culture medium

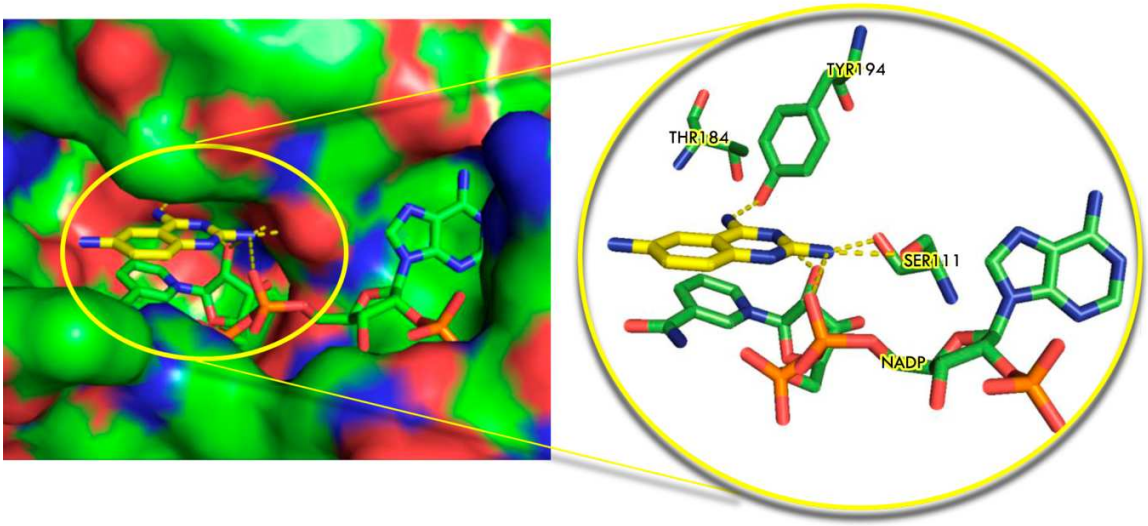

Scheme 1

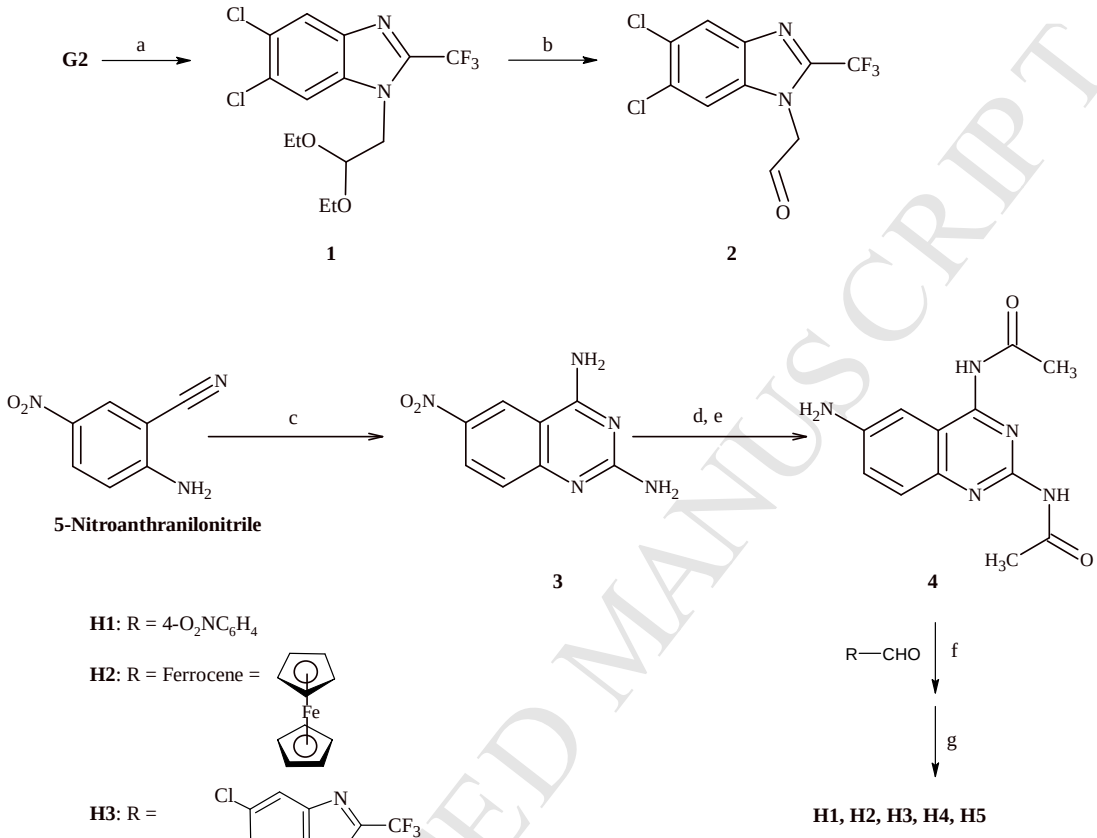

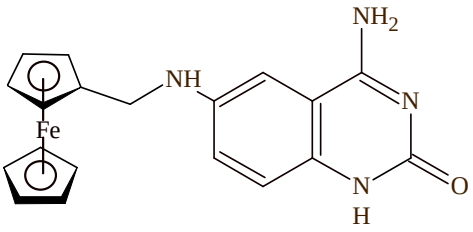

HO2

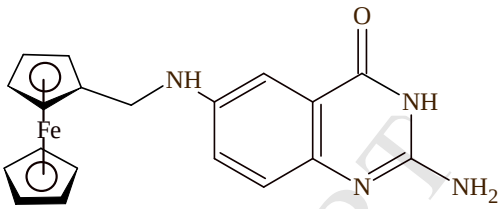

HO4

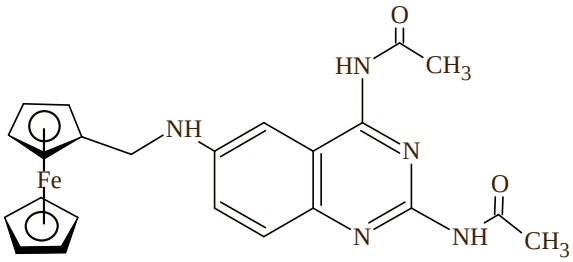

H2A

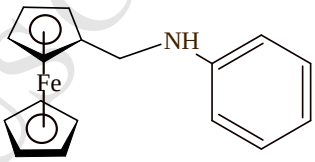

FBC

Scheme 2

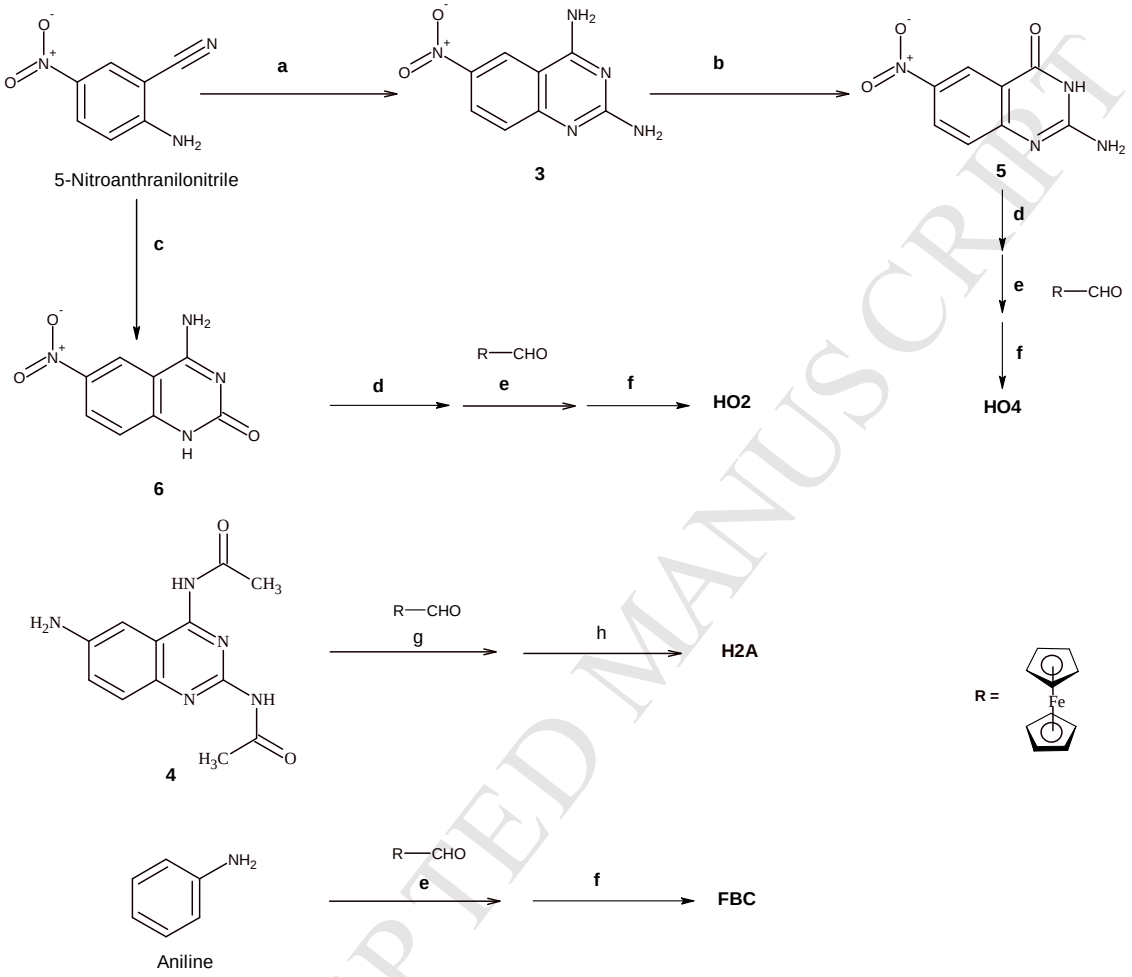

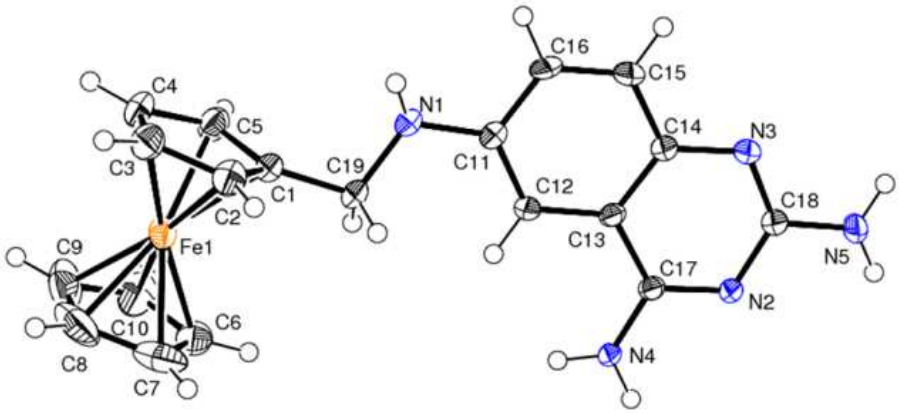

The ethanol solvent molecules were omitted for clarity.

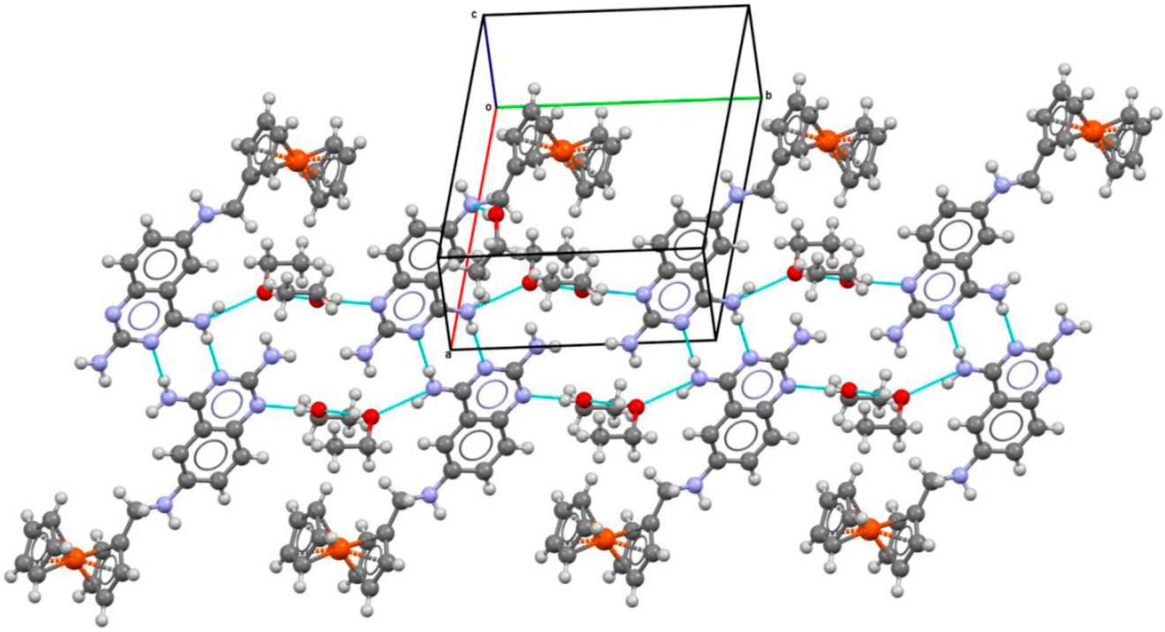

HO4

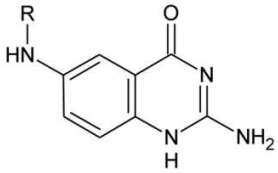

ΔG= 5.34 Kcal

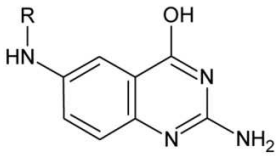

ΔG= 4.48 Kcal

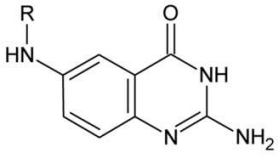

ΔG= 0 Kcal

HO2

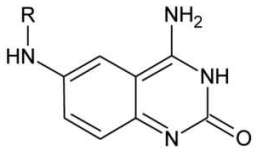

ΔG= 12.28 Kcal

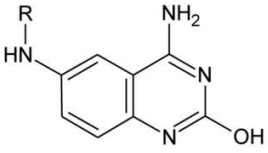

ΔG= 2.45 Kcal

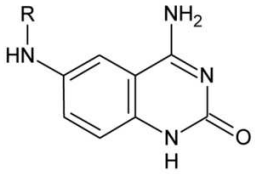

ΔG= 0 Kcal

ΔG value calculated tautomer with the B3LYP 6-31G basis set**

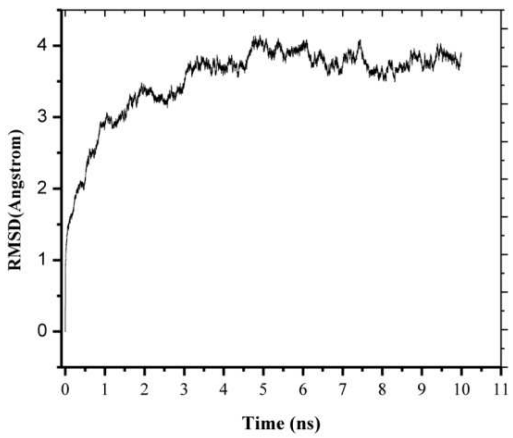

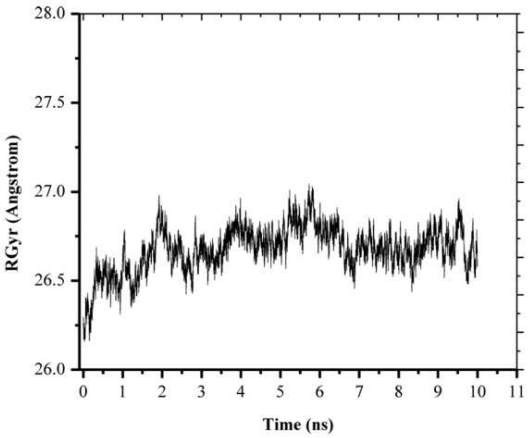

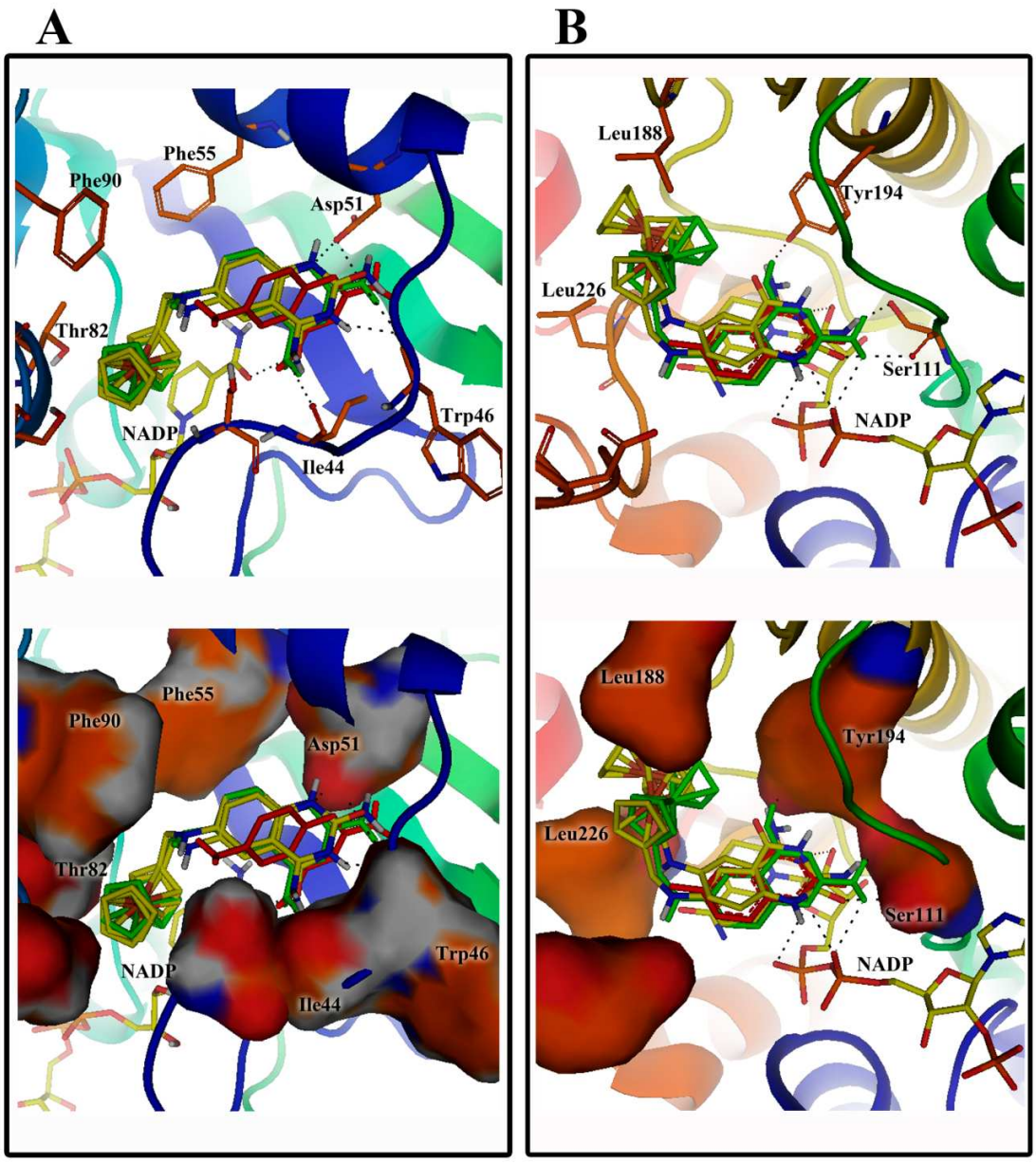

Compound **H2** (green color) interacts similarly to the other compounds.

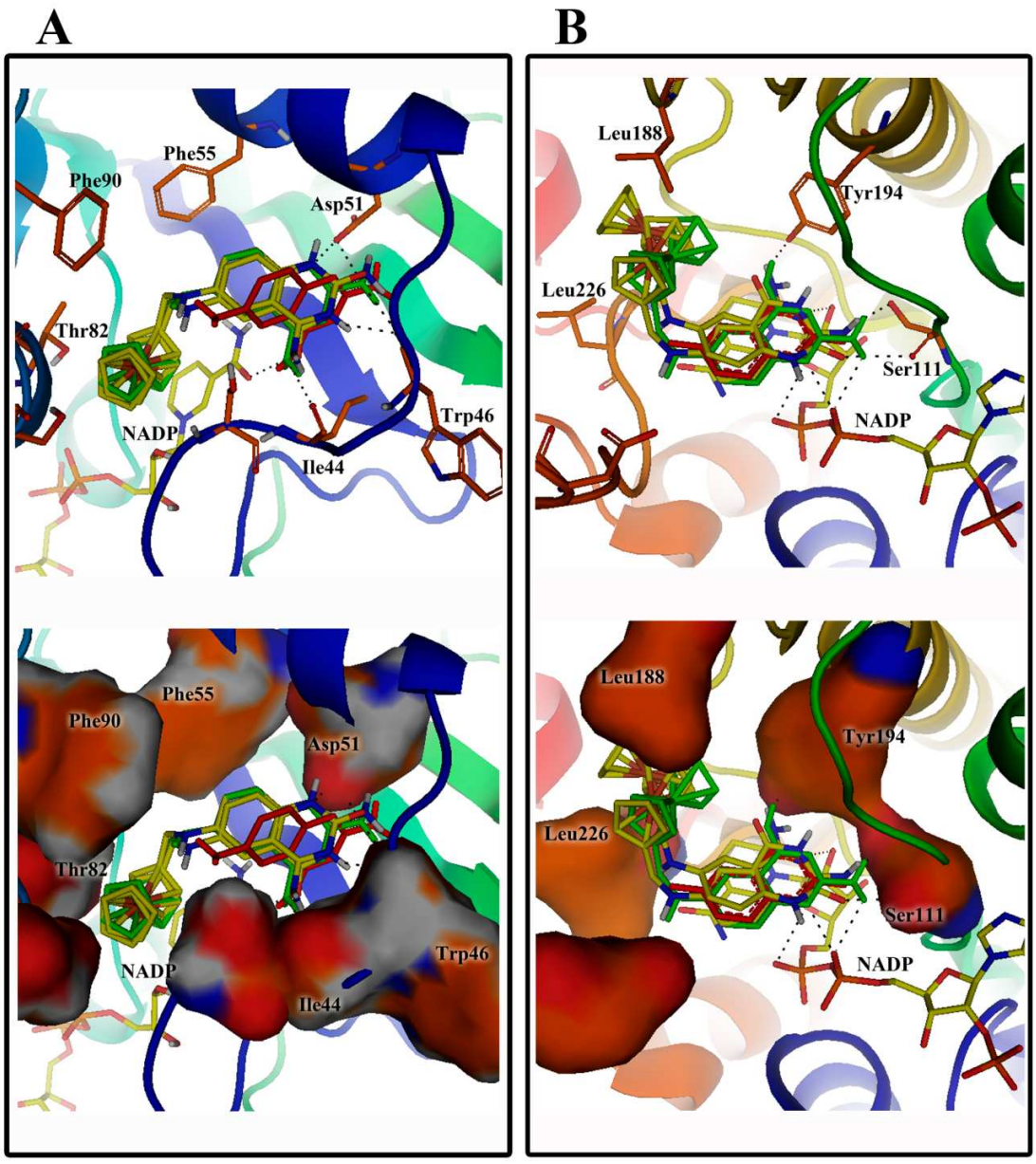

Compound **H2** (green color) interacts similarly to the other compounds.

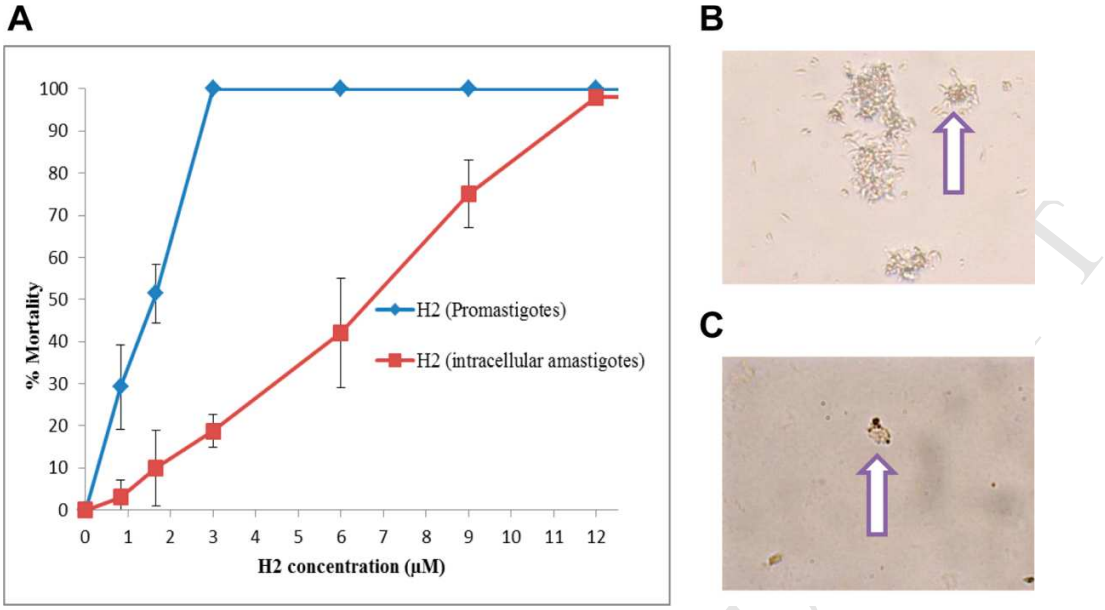

(A) Mortality of promastigotes and amastigotes by **H2**. (B) Microscopic view of the re-cultivation of the macrophages in which the promastigotes are observed outside the macrophages; (C) macrophages infected treated with **H2** at 25 µM. The arrows indicate the macrophages.

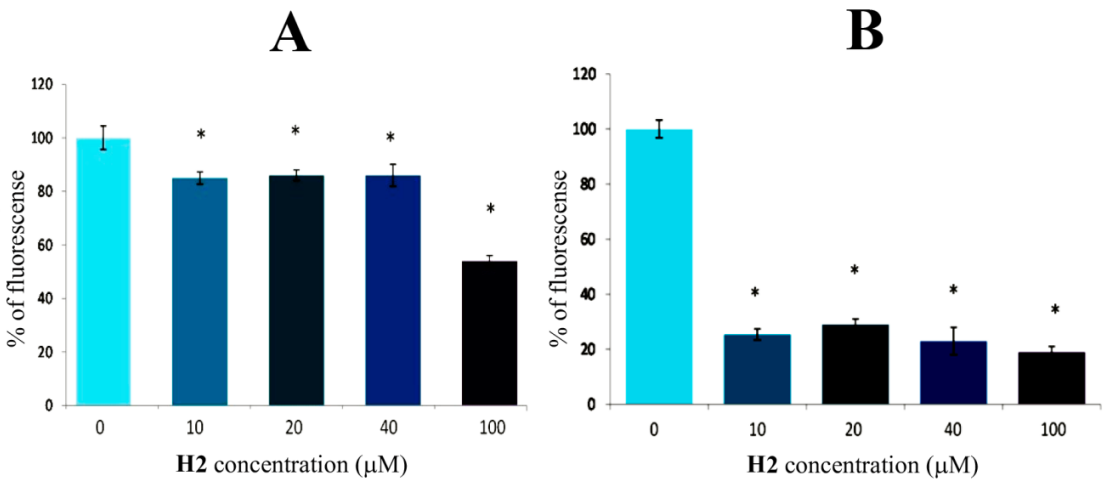

L. mexicana (5 X10 ^{6}) treated with different concentrations of **H2** (0-100 µM) during 1h (A) and 2h (B) before the determinations. The data represent the percentage of fluorescence; the control was considered 100%. At least four independent experiments were performed. * $p<0.05$ vs control without the drug. (Tukey Test). A. U.

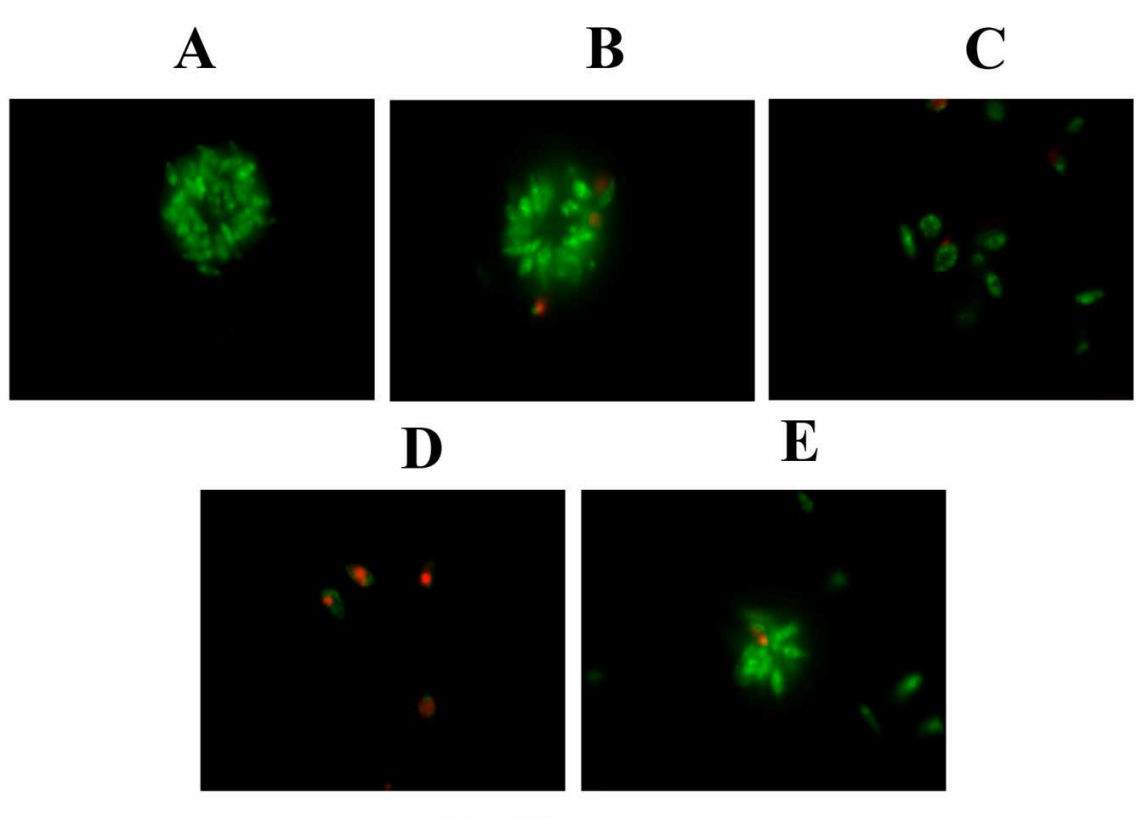

(A) 10 µM, (B) 20 µM, (C) 40 µM, and (D) 100 µM. Although an intense fluorescence with the parasites continued to be observed, some of them had little movement; note that some of the promastigotes were completely immobile. The promastigotes that were less fluorescent and also tested positive for propidium iodide (E).

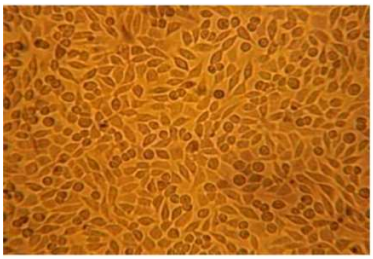

Control (Rank 0)

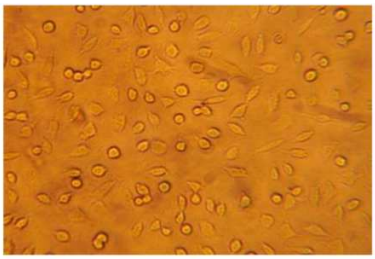

Positive control USP (Rank 4)

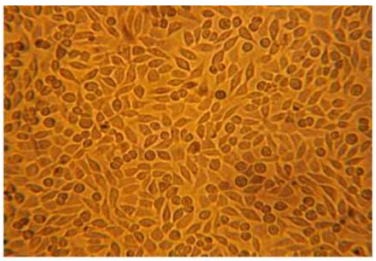

Water: DMSO 99:1 (Rank 1)

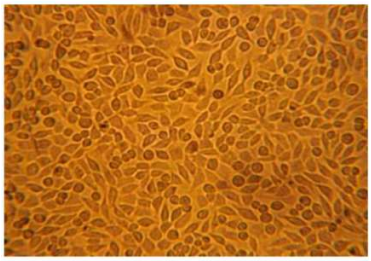

Pyrimethamine-100 µM
(Rank 1)

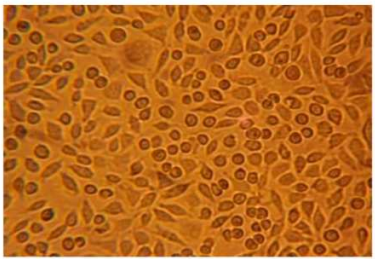

H2-100 µM
(Rank 1)

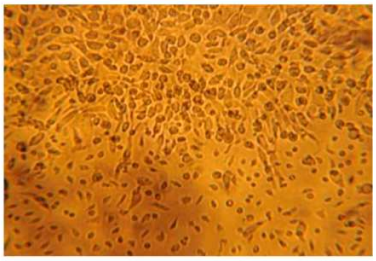

Nifurtimox-100 µM
(Rank 2)

Rank	Reactivity	Description of reactivity
0	none	No detectable zone around or under specimen.
1	slight	Some malformed or degenerated cells under specimen.
2	mild	Zone limited to area under specimen
3	moderate	Zone extend 0.5 to 1.0 cm beyond specimen.
4	severe	Zone extend greater than 1.0 cm beyond specimen.

A

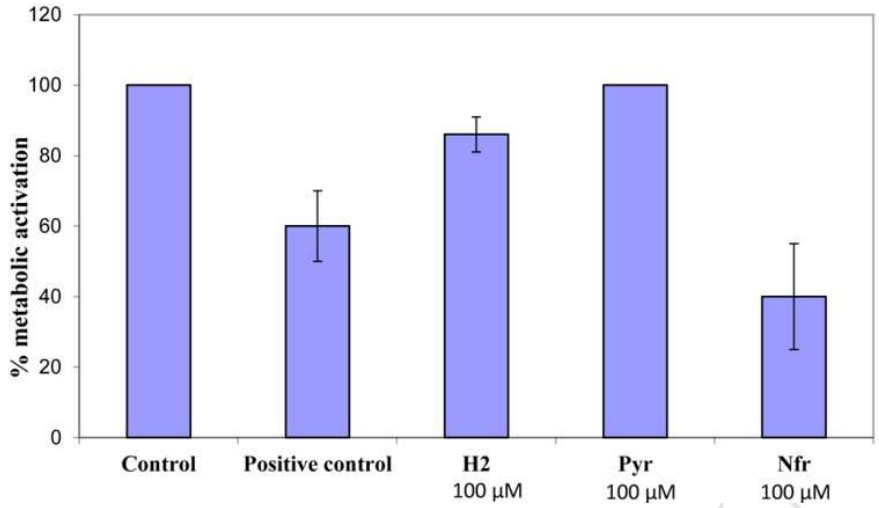

B

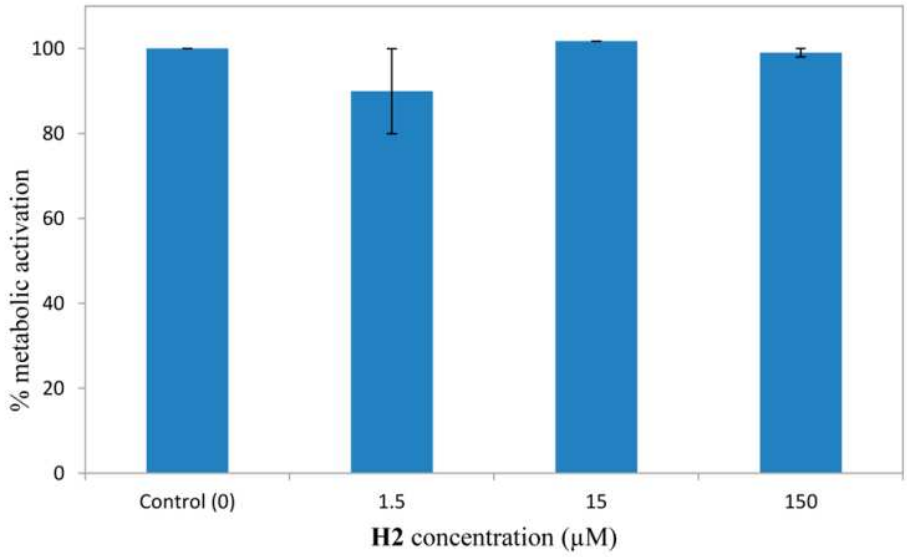

A. Toxicity on was L929, fibroblast cell; **B**. Toxicity on peritoneal macrophages from BALB/c mice. Experiments were carried out in triplicate and repeated at least twice.

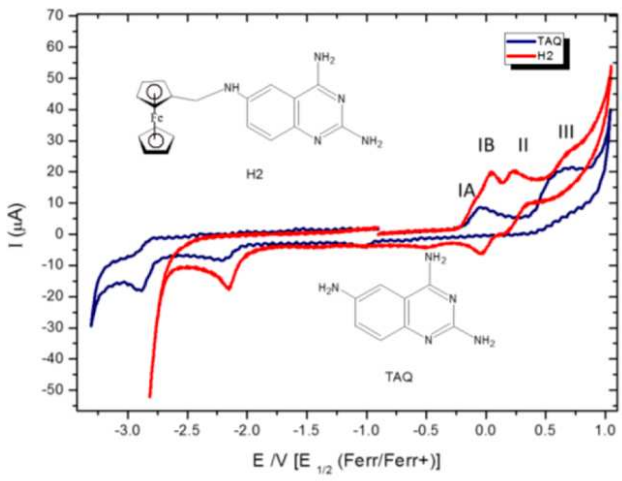

A

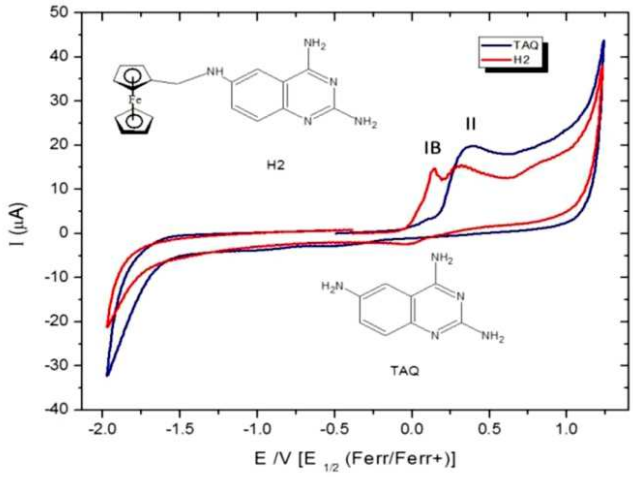

B

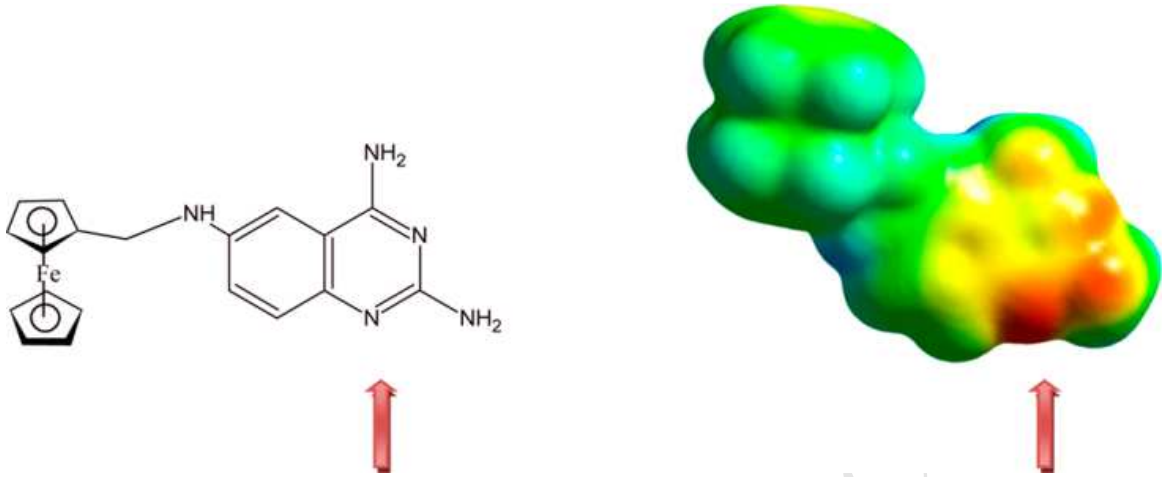

The arrows indicate the position in which there is the greatest electron density

A quinazoline derivative (**H2**) as antileishmanial agent with low citotxicity was find.

H2 is active against promastigote and amastigote form of *Leishmania mexicana.*

H2 begins its antiparasitic action in less than 1 h, probably by oxidative mechanism.

H2 probably has a dual mechanism: oxidative stress inductor and DHFR inhibitors.

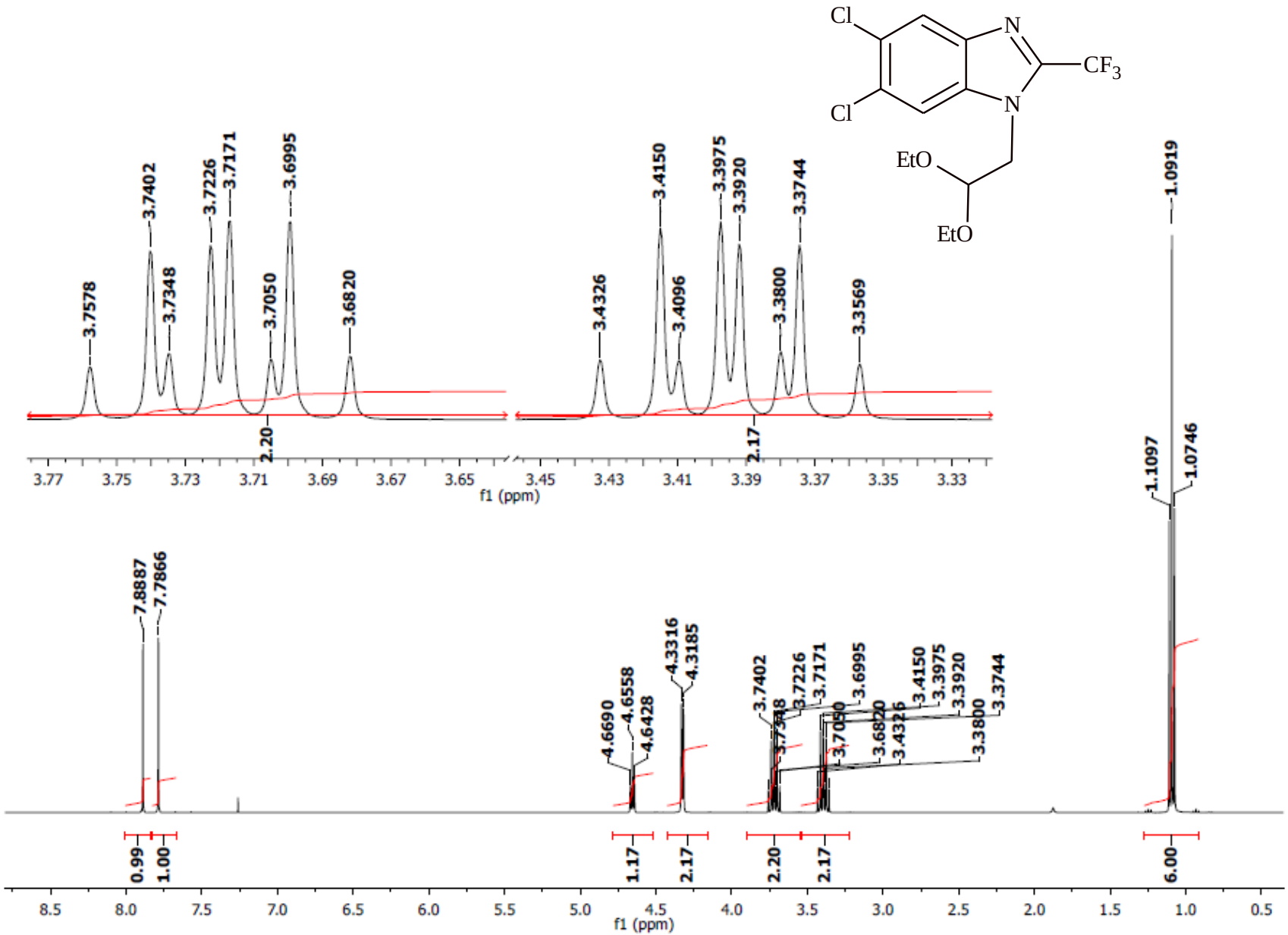
Cl
N
CF3
Cl
N
EtO
EtO
3.7578
3.7402
3.7348
3.7226
3.7171
3.7050
3.6995
3.6820
3.4326
3.4150
3.4096
3.3975
3.3920
3.3800
3.3744
3.3569
2.20
2.17
3.77 3.75 3.73 3.71 3.69 3.67 3.65 3.45 3.43 3.41 3.39 3.37 3.35 3.33
f1 (ppm)
7.8887
7.7866
4.6690
4.6558
4.6428
4.3316
4.3185
1.0919
1.1097
1.0746
0.99
1.00
1.17
2.17
2.20
2.17
6.00
8.5 8.0 7.5 7.0 6.5 6.0 5.5 5.0 4.5 4.0 3.5 3.0 2.5 2.0 1.5 1.0 0.5
f1 (ppm)

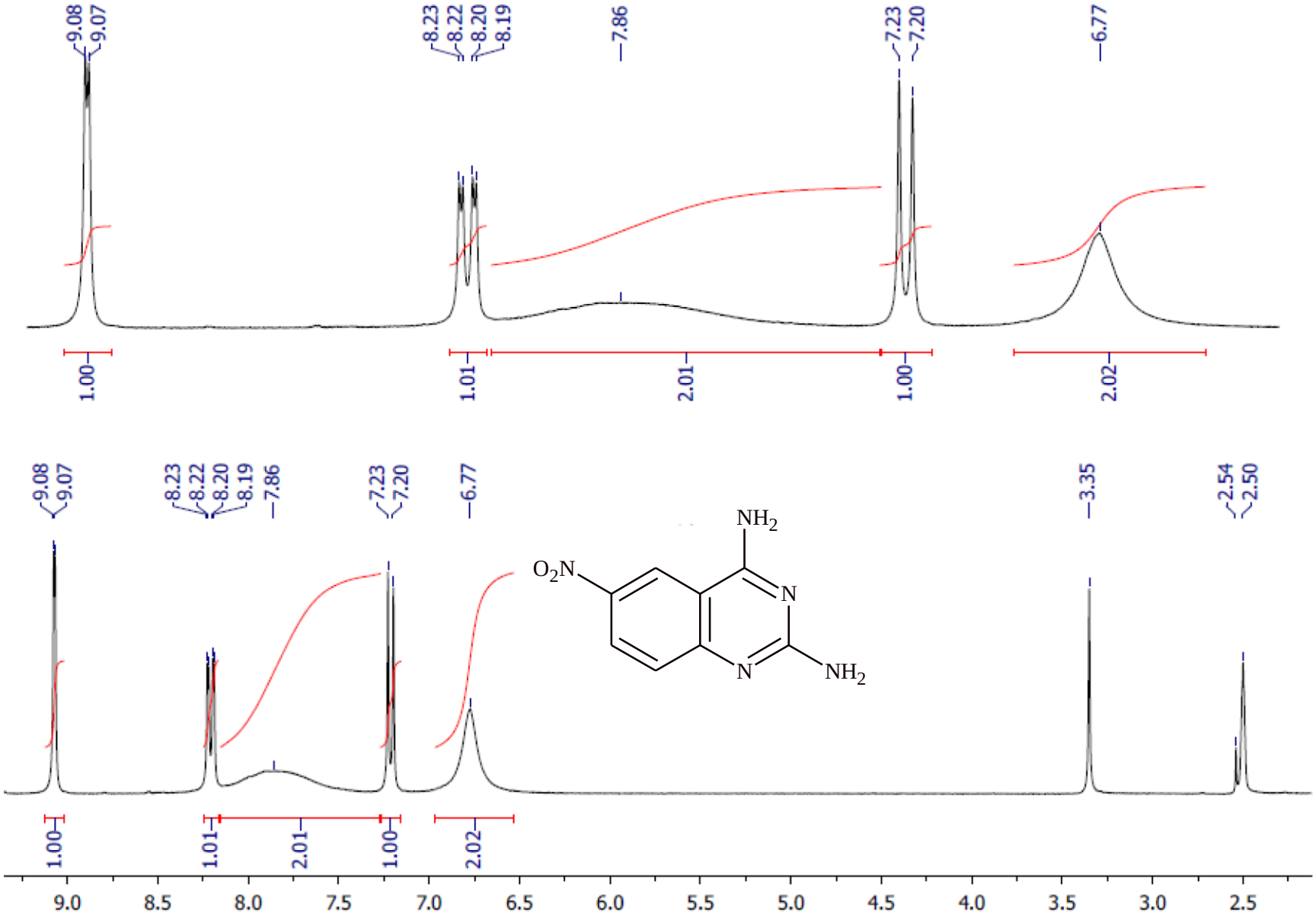
9.08
9.07
8.23
8.22
8.20
8.19
7.86
7.23
7.20
6.77
3.35
2.54
2.50
1.00
1.01
2.01
1.00
2.02
NH2
O2N
N
N
NH2
9.0
8.5
8.0
7.5
7.0
6.5
6.0
5.5
5.0
4.5
4.0
3.5
3.0
2.5

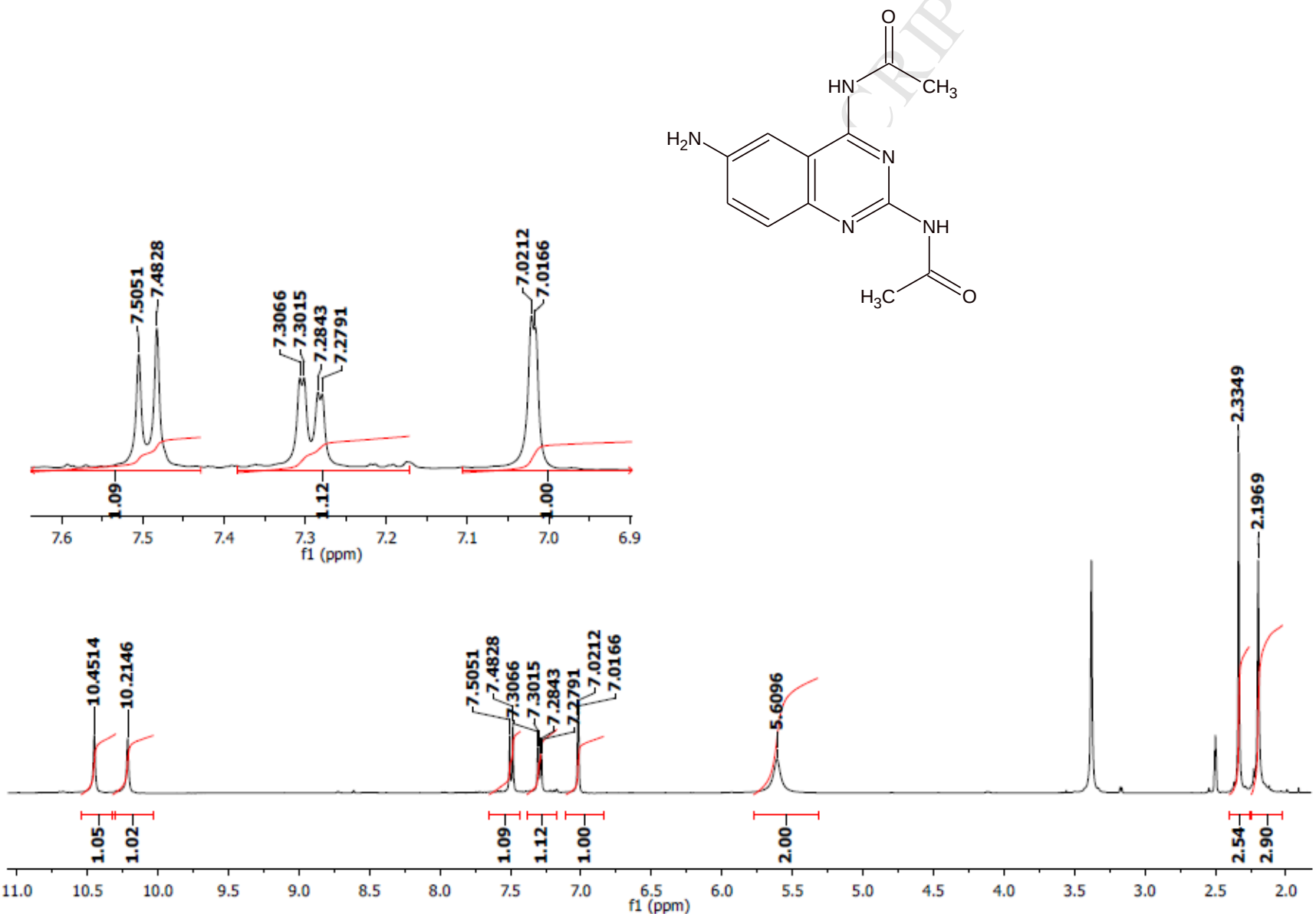
O
HN
CH3
H2N
N
N
NH
H3C
O
7.5051
7.4828
7.3066
7.3015
7.2843
7.2791
7.0212
7.0166
1.09
1.12
1.00
7.6
7.5
7.4
7.3
7.2
7.1
7.0
6.9
f1 (ppm)
10.4514
10.2146
7.5051
7.4828
7.3066
7.3015
7.2843
7.2791
7.0212
7.0166
5.6096
2.3349
2.1969
1.05
1.02
1.09
1.12
1.00
2.00
2.54
2.90
11.0
10.5
10.0
9.5
9.0
8.5
8.0
7.5
7.0
6.5
6.0
5.5
5.0
4.5
4.0
3.5
3.0
2.5
2.0
f1 (ppm)

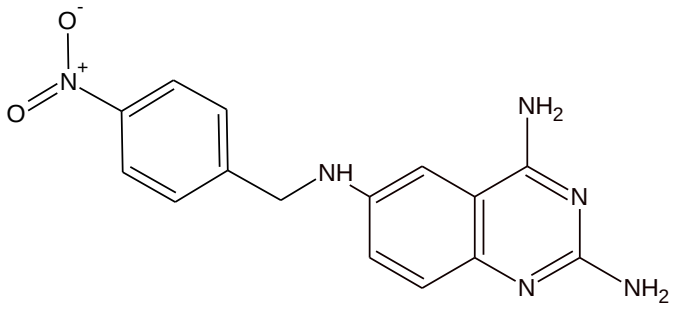
O
N+
O
NH
NH2
N
N
NH2

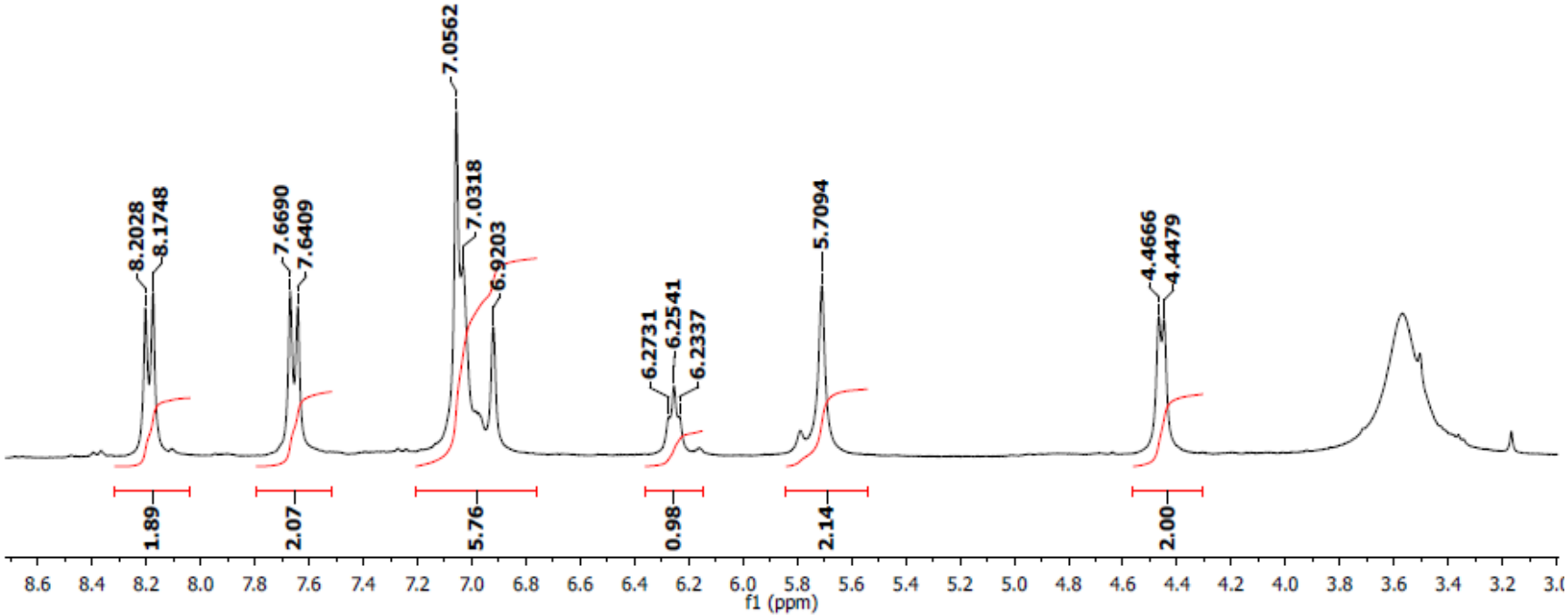
8.2028
8.1748
7.6690
7.6409
7.0562
7.0318
6.9203
6.2731
6.2541
6.2337
5.7094
4.4666
4.4479
1.89
2.07
5.76
0.98
2.14
2.00
8.6 8.4 8.2 8.0 7.8 7.6 7.4 7.2 7.0 6.8 6.6 6.4 6.2 6.0 5.8 5.6 5.4 5.2 5.0 4.8 4.6 4.4 4.2 4.0 3.8 3.6 3.4 3.2
f1 (ppm)

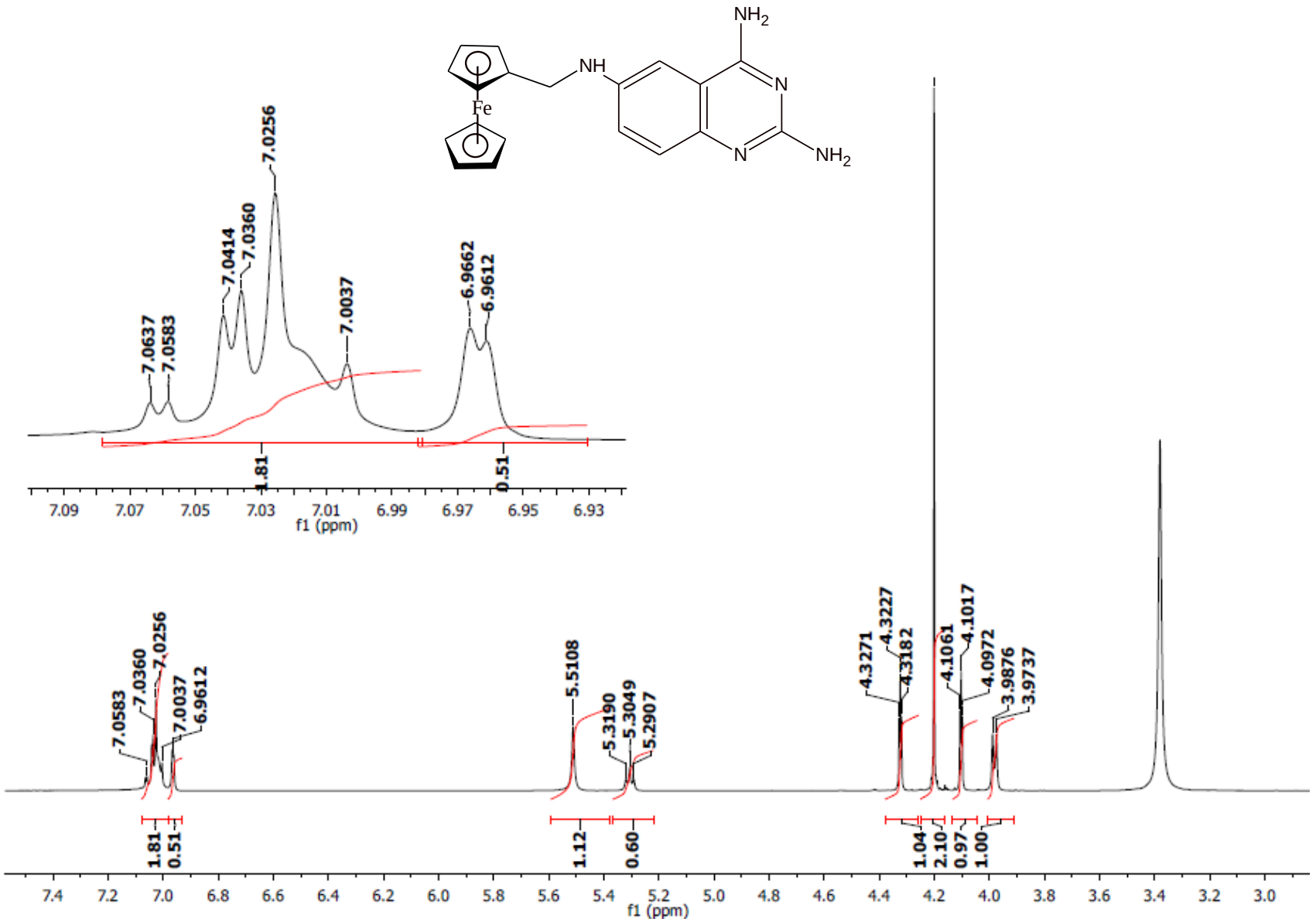
NH2
NH
N
Fe
N
NH2
7.0637
7.0583
7.0414
7.0360
7.0256
7.0037
6.9662
6.9612
1.81
0.51
7.09
7.07
7.05
7.03
7.01
6.99
6.97
6.95
6.93
f1 (ppm)
7.0583
7.0360
7.0256
7.0037
6.9612
5.5108
5.3190
5.3049
5.2907
4.3271
4.3227
4.3182
4.1061
4.1017
4.0972
3.9876
3.9737
1.81
0.51
1.12
0.60
1.04
2.10
0.97
1.00
7.4
7.2
7.0
6.8
6.6
6.4
6.2
6.0
5.8
5.6
5.4
5.2
5.0
4.8
4.6
4.4
4.2
4.0
3.8
3.6
3.4
3.2
3.0
f1 (ppm)

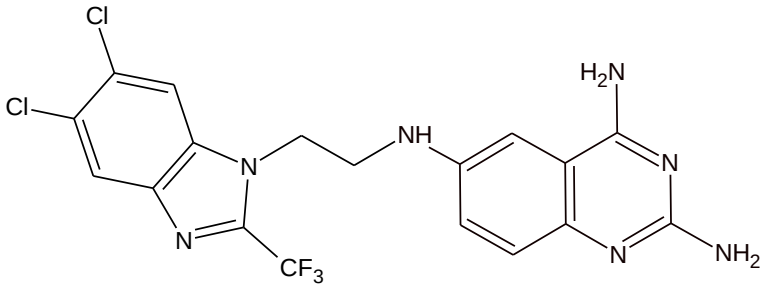
Cl
Cl
N
N
CF3
NH
H2N
N
N
NH2

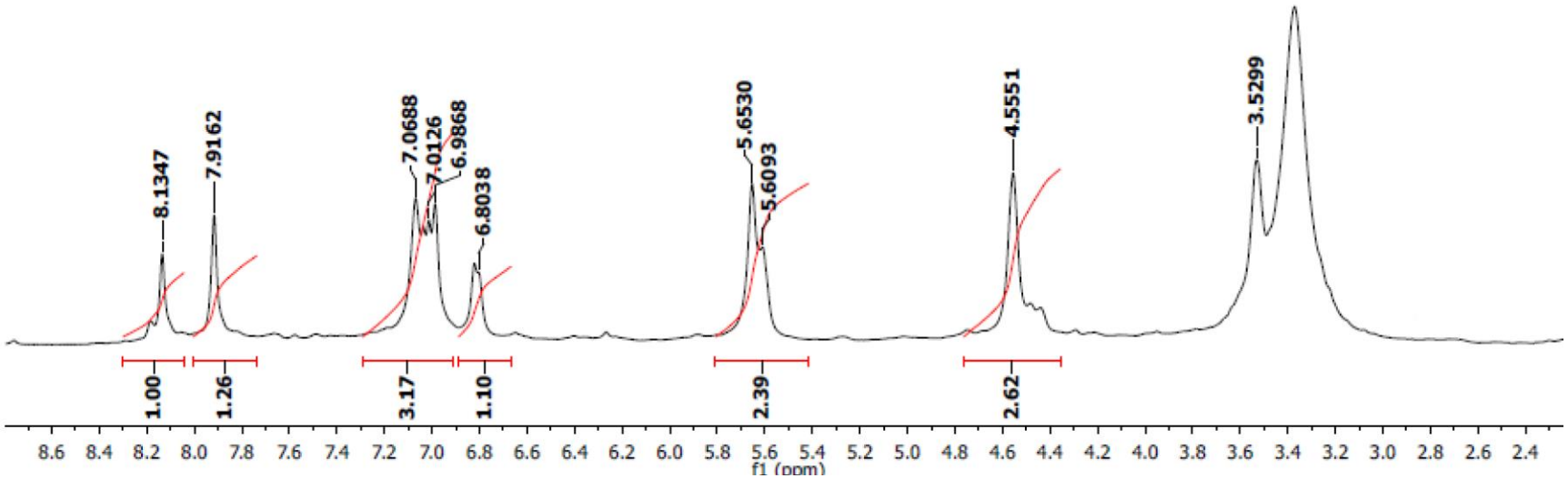
8.1347
7.9162
7.0688
7.0126
6.9868
6.8038
5.6530
5.6093
4.5551
3.5299
1.00
1.26
3.17
1.10
2.39
2.62
8.6 8.4 8.2 8.0 7.8 7.6 7.4 7.2 7.0 6.8 6.6 6.4 6.2 6.0 5.8 5.6 5.4 5.2 5.0 4.8 4.6 4.4 4.2 4.0 3.8 3.6 3.4 3.2 3.0 2.8 2.6 2.4
f1 (ppm)

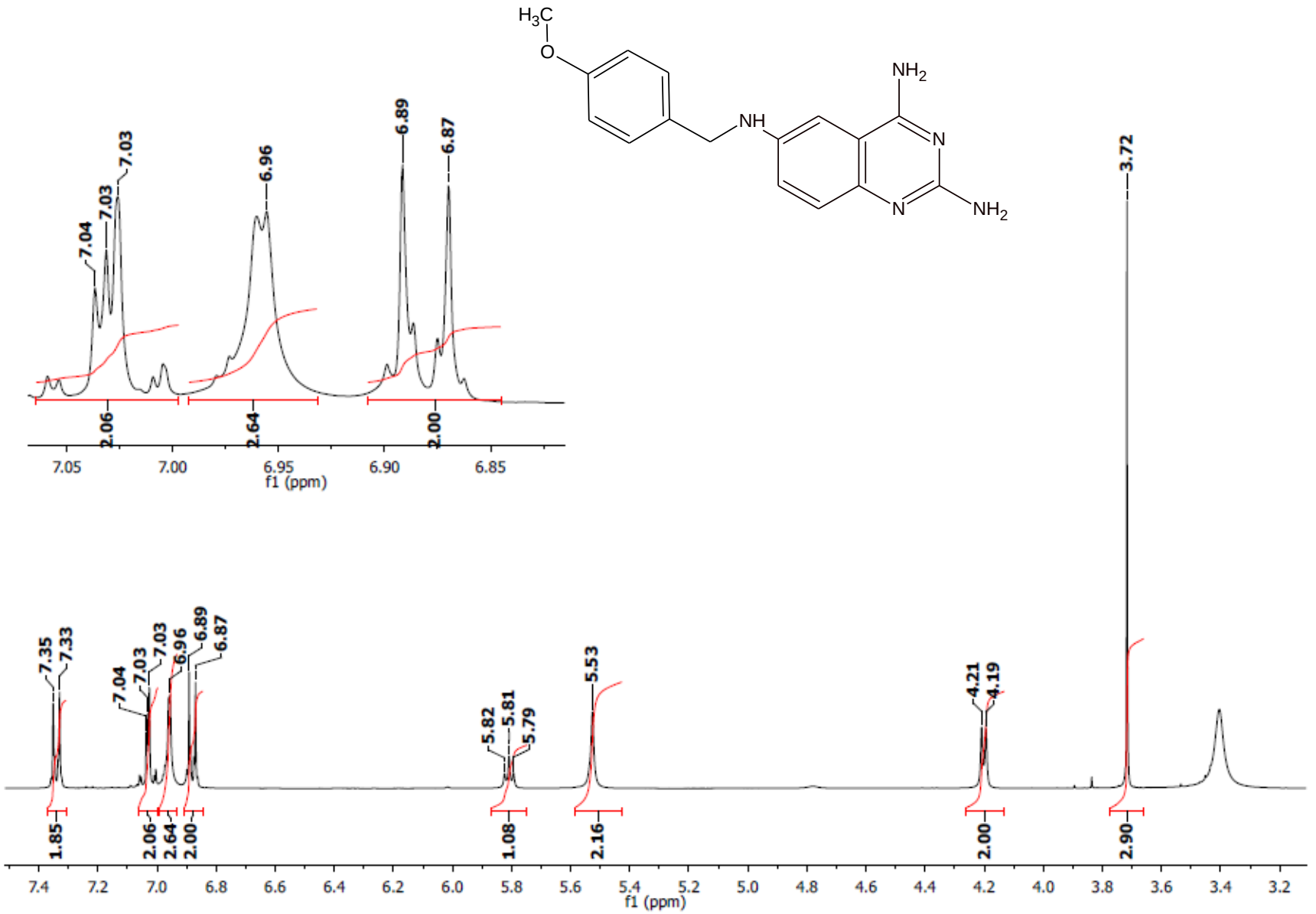
H3C
O
NH
NH2
N
N
NH2
7.04
7.03
7.03
6.96
6.89
6.87
2.06
2.64
2.00
7.05
7.00
6.95
6.90
6.85
f1 (ppm)
7.35
7.33
7.04
7.03
7.03
6.96
6.89
6.87
5.82
5.81
5.79
5.53
4.21
4.19
3.72
1.85
2.06
2.64
2.00
1.08
2.16
2.00
2.90
7.4
7.2
7.0
6.8
6.6
6.4
6.2
6.0
5.8
5.6
5.4
5.2
5.0
4.8
4.6
4.4
4.2
4.0
3.8
3.6
3.4
3.2
f1 (ppm)

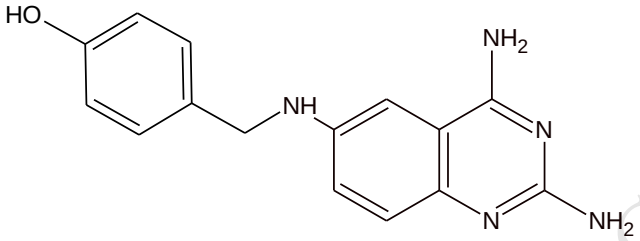
HO
NH
NH2
N
N
NH2

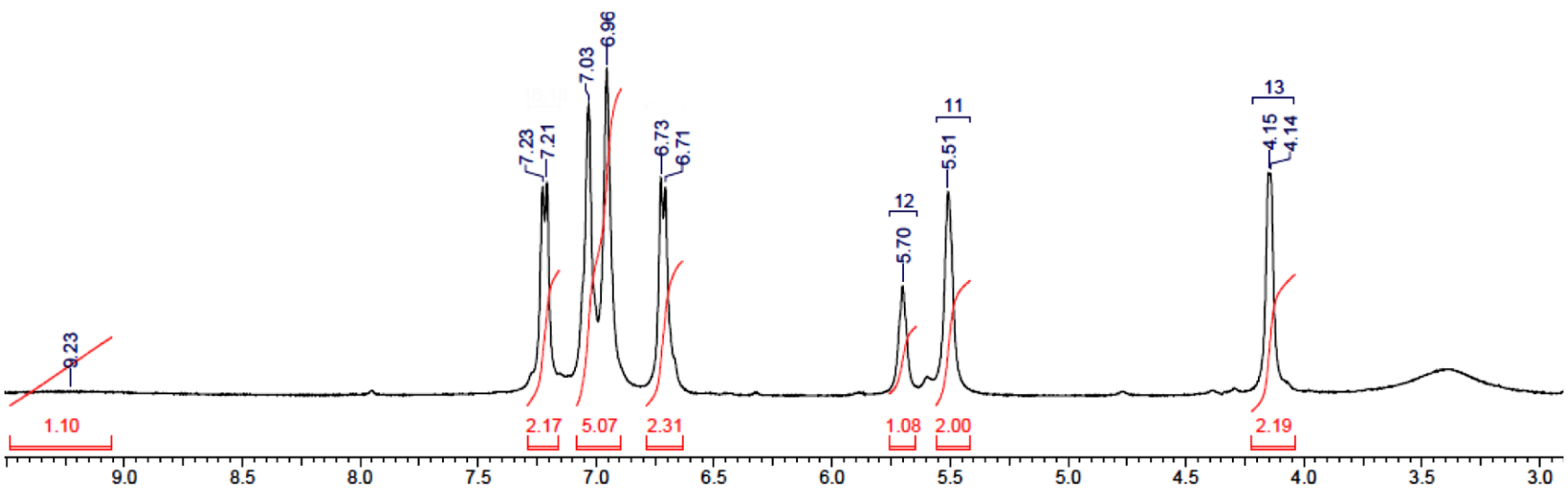
9.23
7.23
7.21
7.03
6.96
6.73
6.71
5.70
5.51
4.15
4.14
1.10
2.17
5.07
2.31
1.08
2.00
2.19
9.0
8.5
8.0
7.5
7.0
6.5
6.0
5.5
5.0
4.5
4.0
3.5
3.0

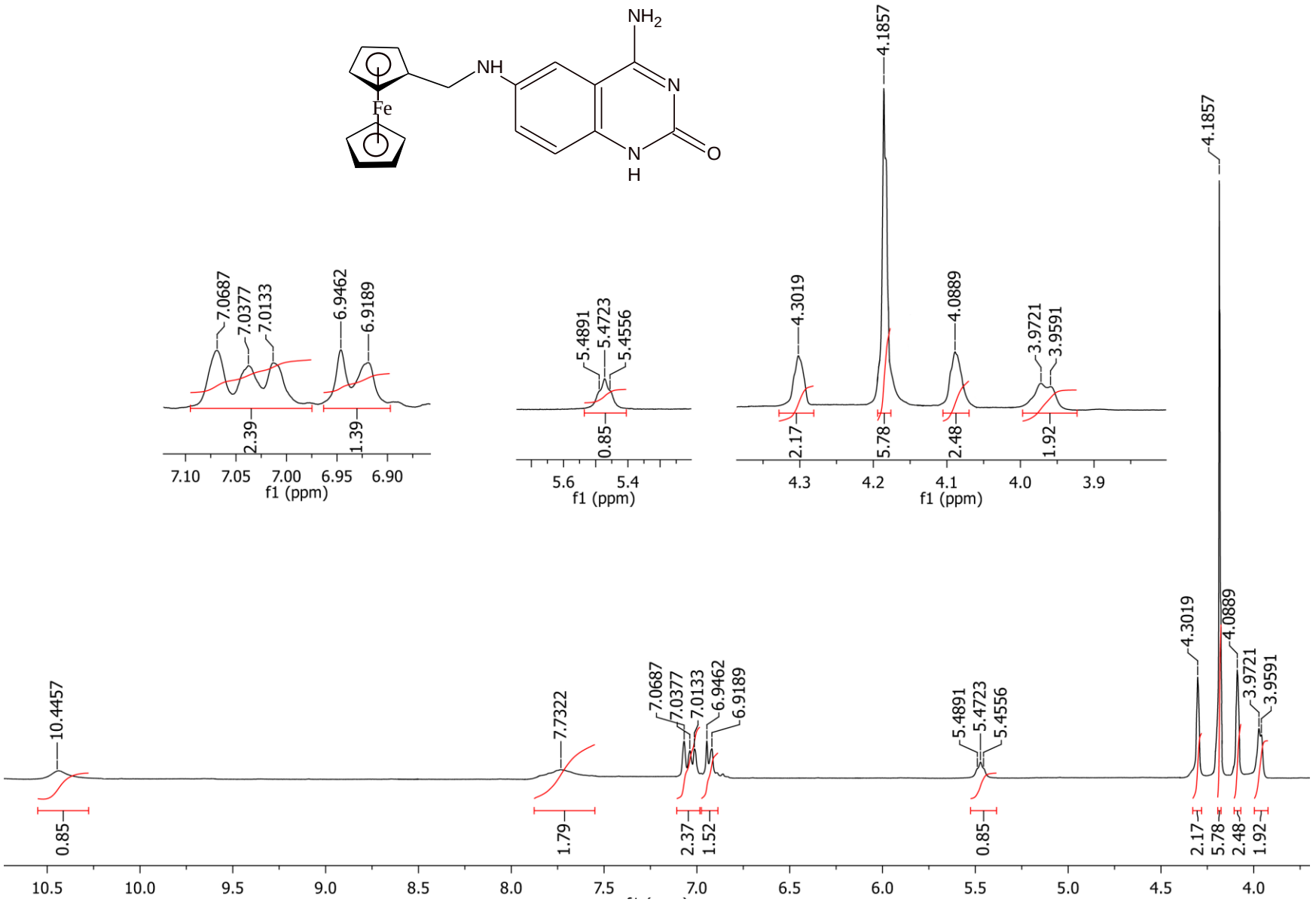
NH2
NH
N
Fe
N
H
O
7.0687
7.0377
7.0133
6.9462
6.9189
2.39
1.39
7.10
7.05
7.00
6.95
6.90
f1 (ppm)
5.4891
5.4723
5.4556
0.85
5.6
5.4
f1 (ppm)
4.3019
4.1857
4.0889
3.9721
3.9591
2.17
5.78
2.48
1.92
4.3
4.2
4.1
4.0
3.9
f1 (ppm)
10.4457
7.7322
7.0687
7.0377
7.0133
6.9462
6.9189
5.4891
5.4723
5.4556
4.3019
4.1857
4.0889
3.9721
3.9591
0.85
1.79
2.37
1.52
0.85
2.17
5.78
2.48
1.92
10.5
10.0
9.5
9.0
8.5
8.0
7.5
7.0
6.5
6.0
5.5
5.0
4.5
4.0

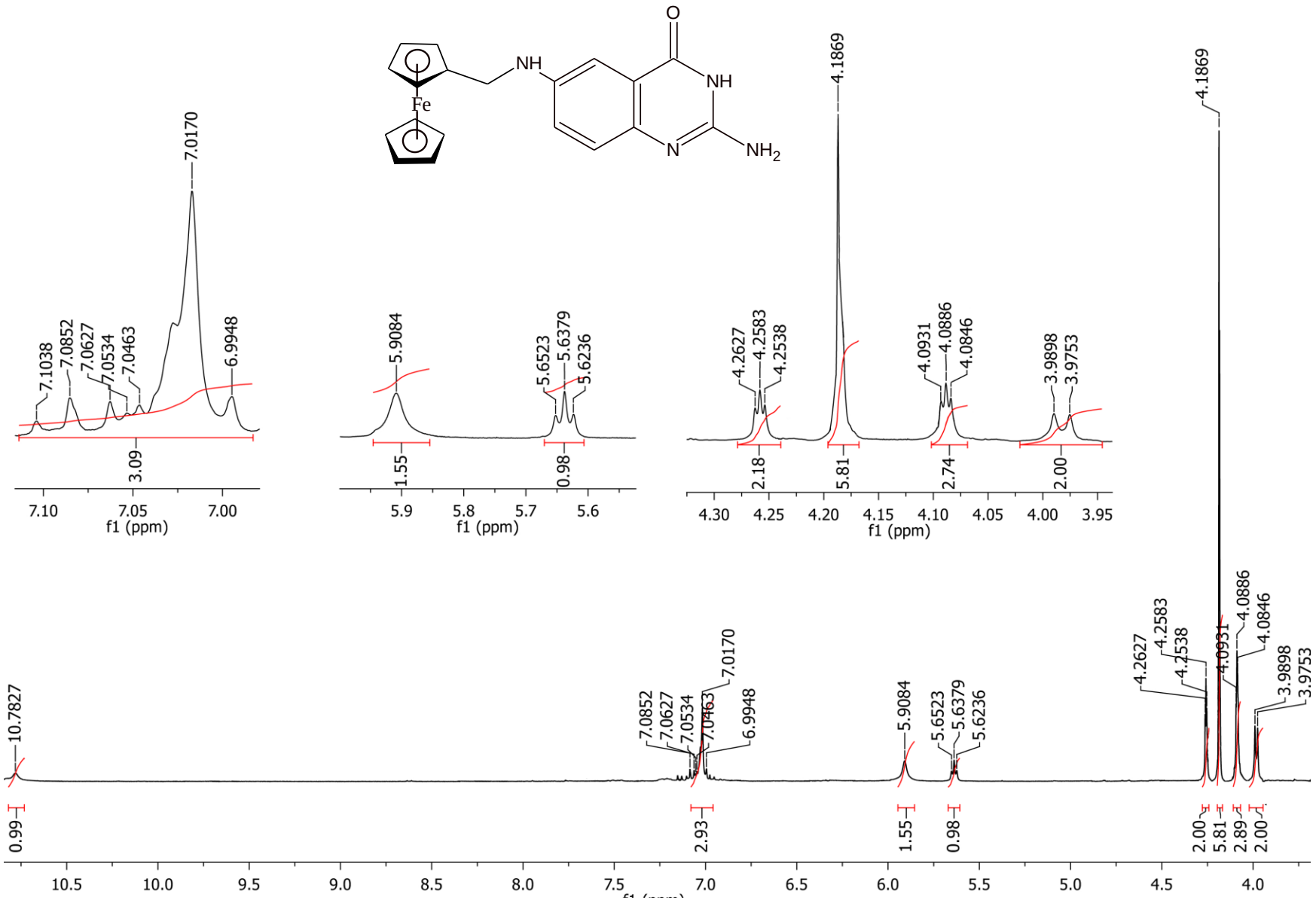
O
NH
NH
Fe
N
NH2
7.1038
7.0852
7.0627
7.0534
7.0463
7.0170
6.9948
3.09
7.10
7.05
7.00
f1 (ppm)
5.9084
5.6523
5.6379
5.6236
1.55
0.98
5.9
5.8
5.7
5.6
f1 (ppm)
4.2627
4.2583
4.2538
4.1869
4.0931
4.0886
4.0846
3.9898
3.9753
2.18
5.81
2.74
2.00
4.30
4.25
4.20
4.15
4.10
4.05
4.00
3.95
f1 (ppm)
10.7827
7.0852
7.0627
7.0534
7.0463
7.0170
6.9948
5.9084
5.6523
5.6379
5.6236
4.2627
4.2583
4.2538
4.1869
4.0931
4.0886
4.0846
3.9898
3.9753
0.99
2.93
1.55
0.98
2.00
5.81
2.89
2.00
10.5
10.0
9.5
9.0
8.5
8.0
7.5
7.0
6.5
6.0
5.5
5.0
4.5
4.0

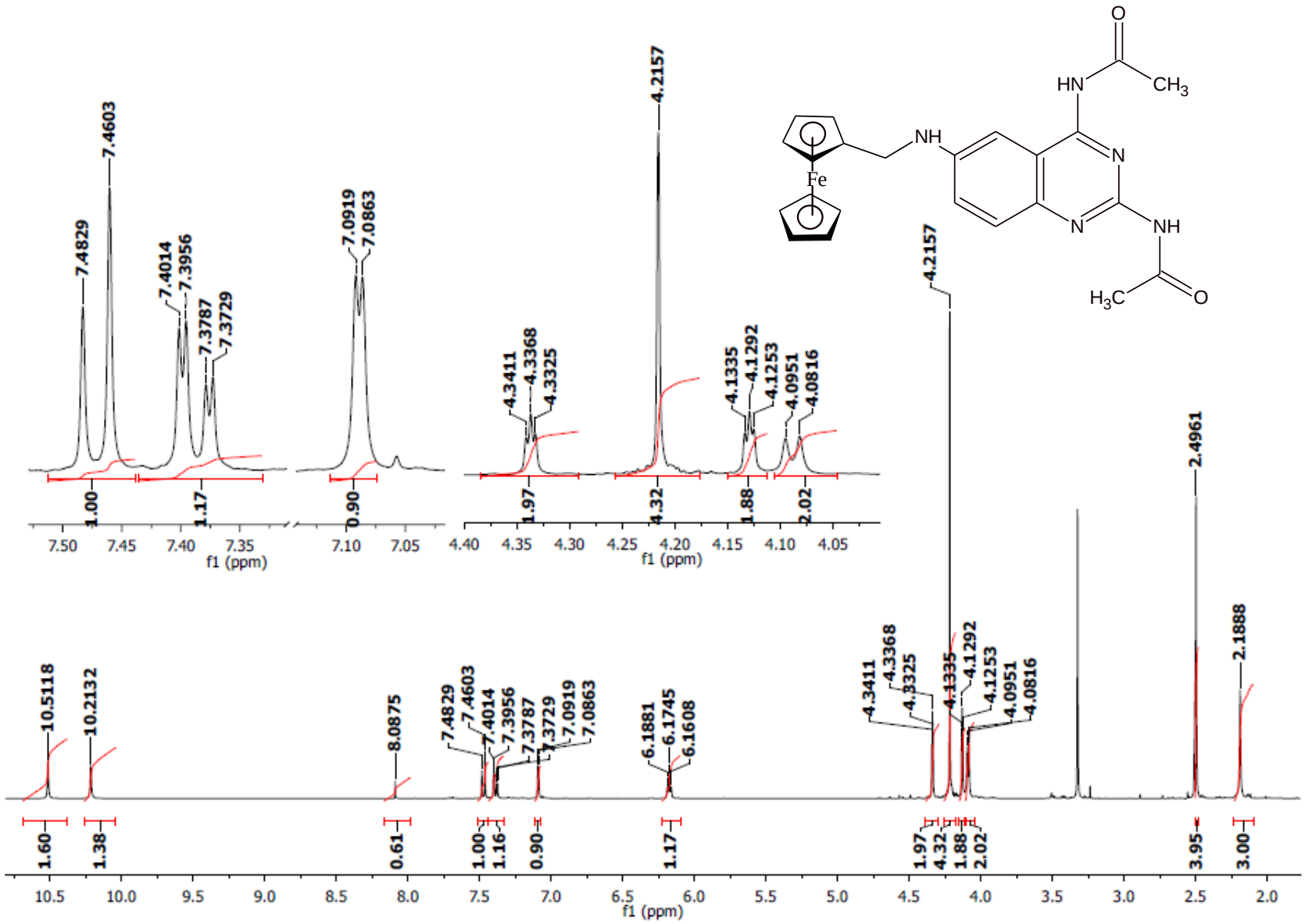
10.5118
10.2132
8.0875
7.4829
7.4603
7.4014
7.3956
7.3787
7.3729
7.0919
7.0863
6.1881
6.1745
6.1608
4.3411
4.3368
4.3325
4.2157
4.1335
4.1292
4.1253
4.0951
4.0816
2.4961
2.1888
1.60
1.38
0.61
1.00
1.16
0.90
1.17
1.97
4.32
1.88
2.02
3.95
3.00
f1 (ppm)
HN
CH3
NH
N
N
NH
Fe
H3C
O

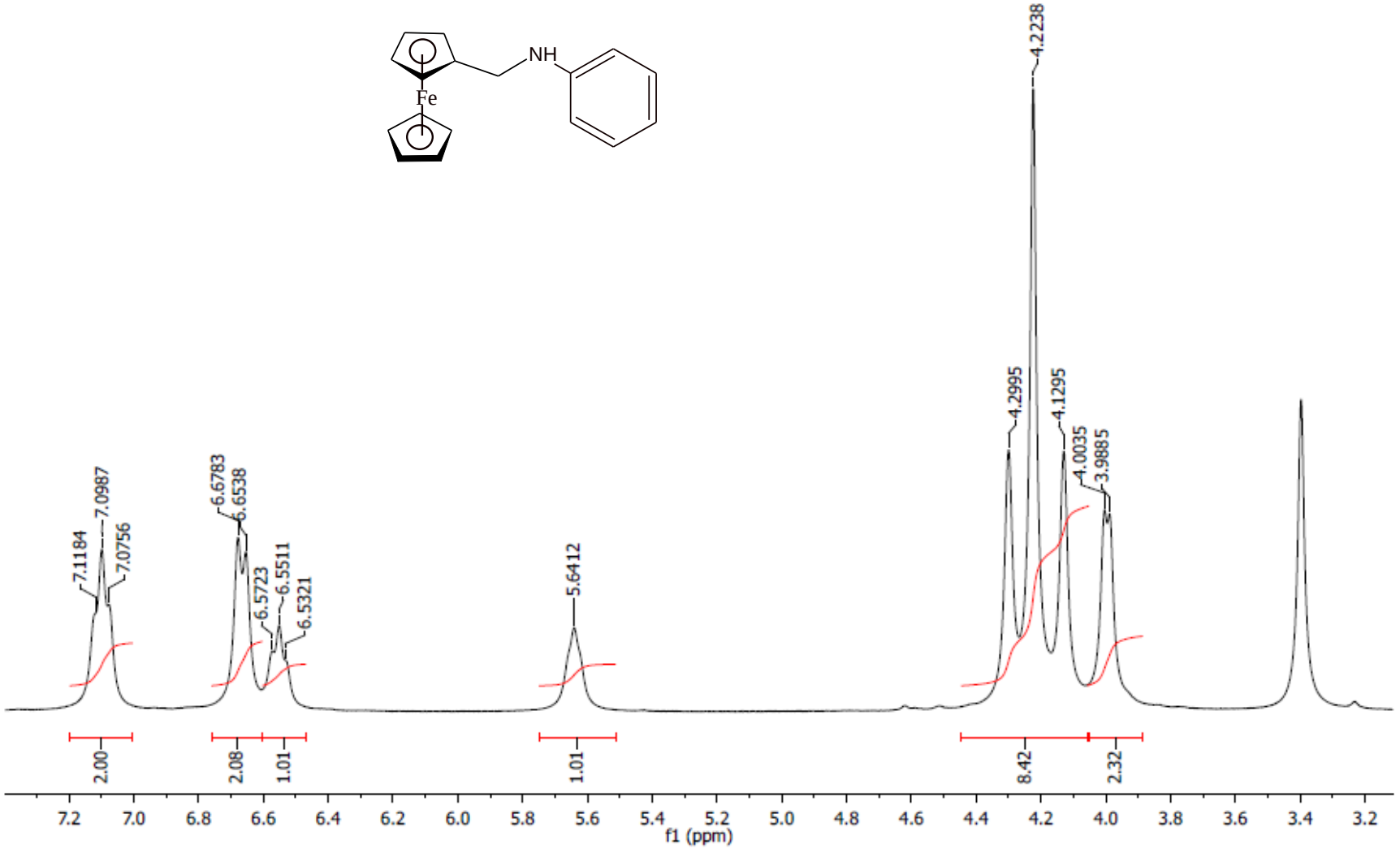
NH
Fe
4.2238
4.2995
4.1295
4.0035
3.9885
7.1184
7.0987
7.0756
6.6783
6.6538
6.5723
6.5511
6.5321
5.6412
2.00
2.08
1.01
1.01
8.42
2.32
7.2
7.0
6.8
6.6
6.4
6.2
6.0
5.8
5.6
5.4
5.2
5.0
4.8
4.6
4.4
4.2
4.0
3.8
3.6
3.4
3.2
f1 (ppm)

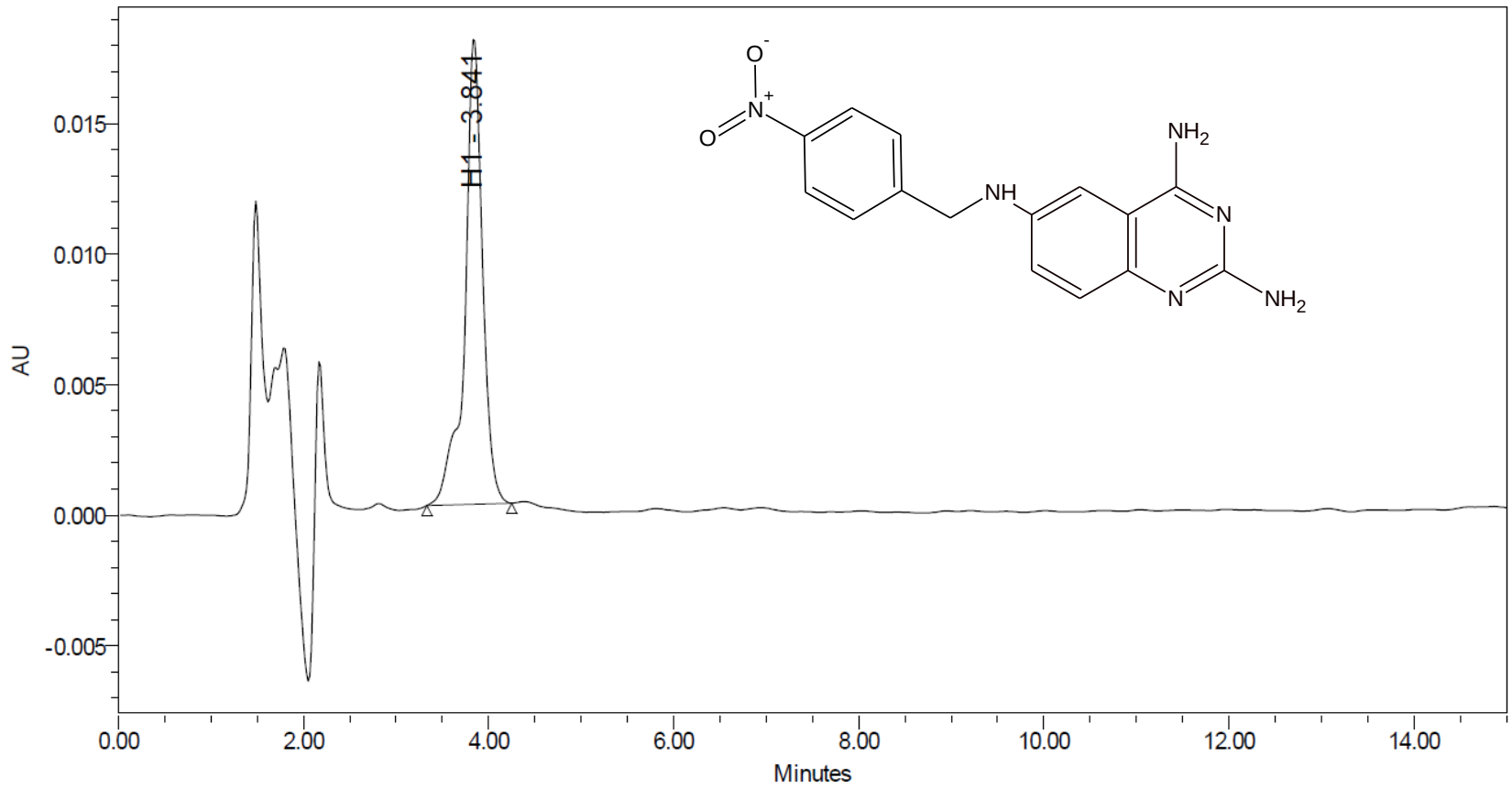

	Peak Name	RT	Area	% Area	Height	% Height	Units
1	H1	3.841	237271	100.00	17897	100.00	µg/mL

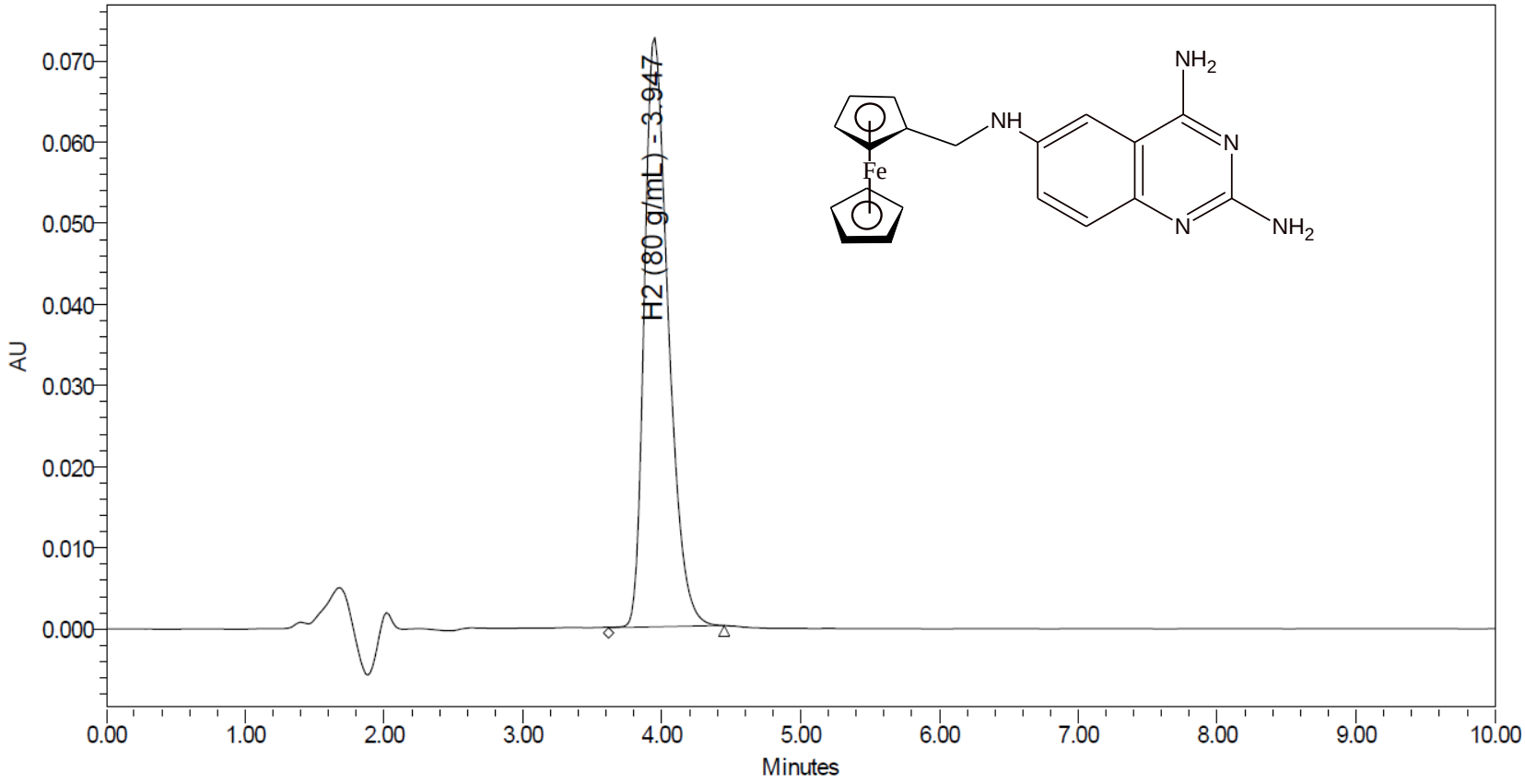

	Peak Name	RT	Area	% Area	Height	% Height
1	H2 (80 g/mL)	3.947	873732	100.00	72681	100.00

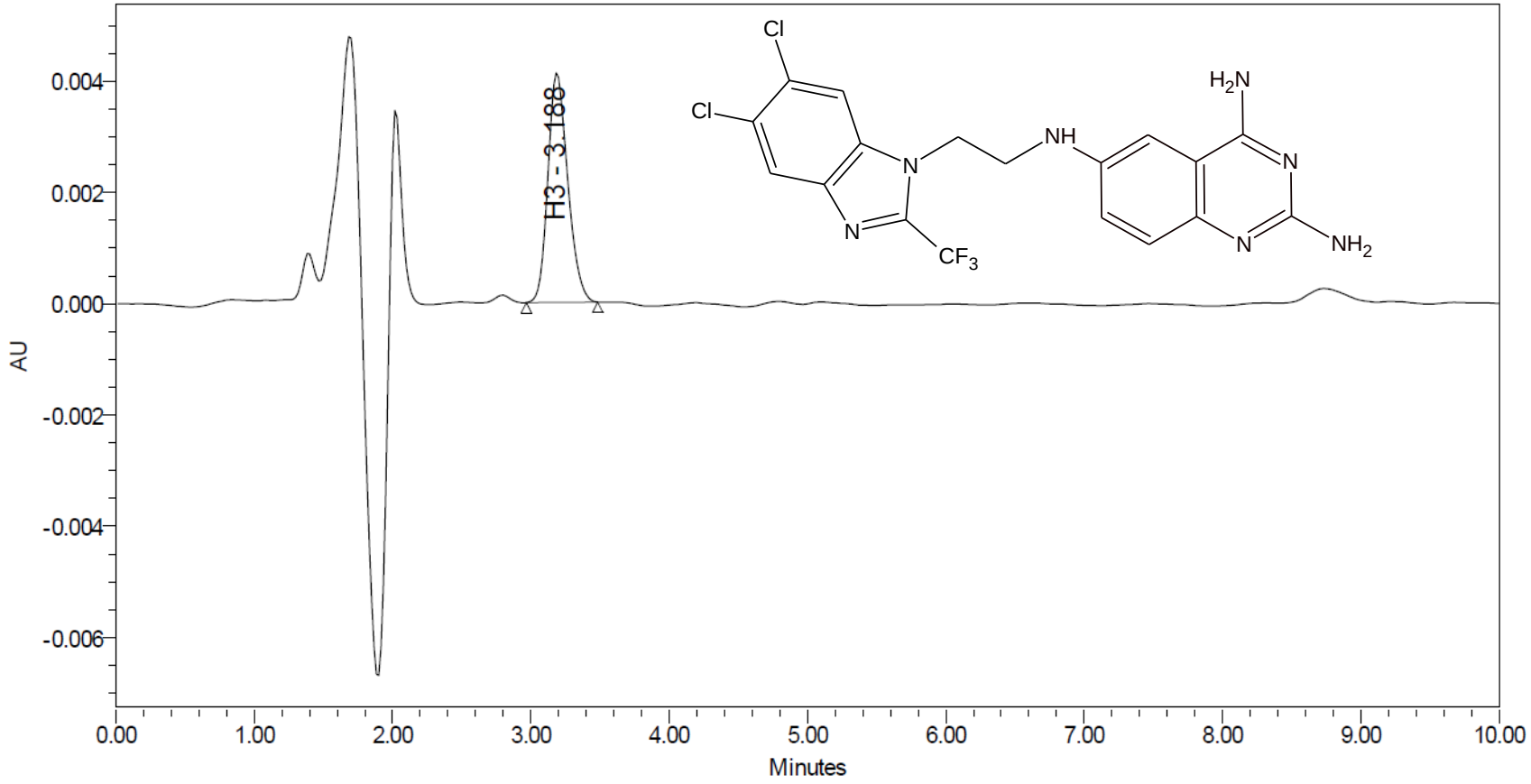

	Peak Name	RT	Area	% Area	Height	% Height	Units
1	H3	3.188	41127	100.00	4131	100.00	µg/mL

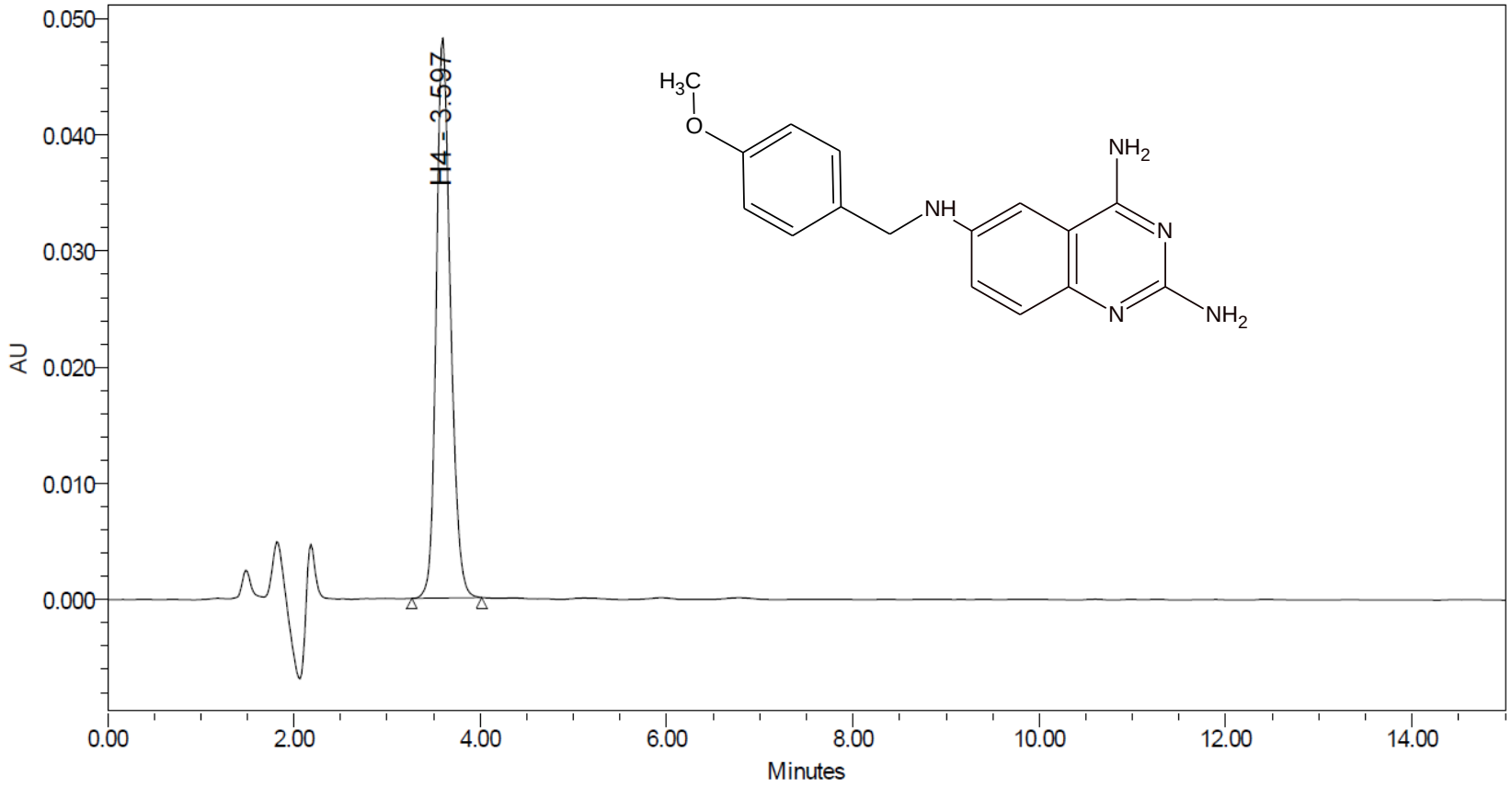

	Peak Name	RT	Area	% Area	Height	% Height
1	H4	3.597	510793	100.00	48227	100.00

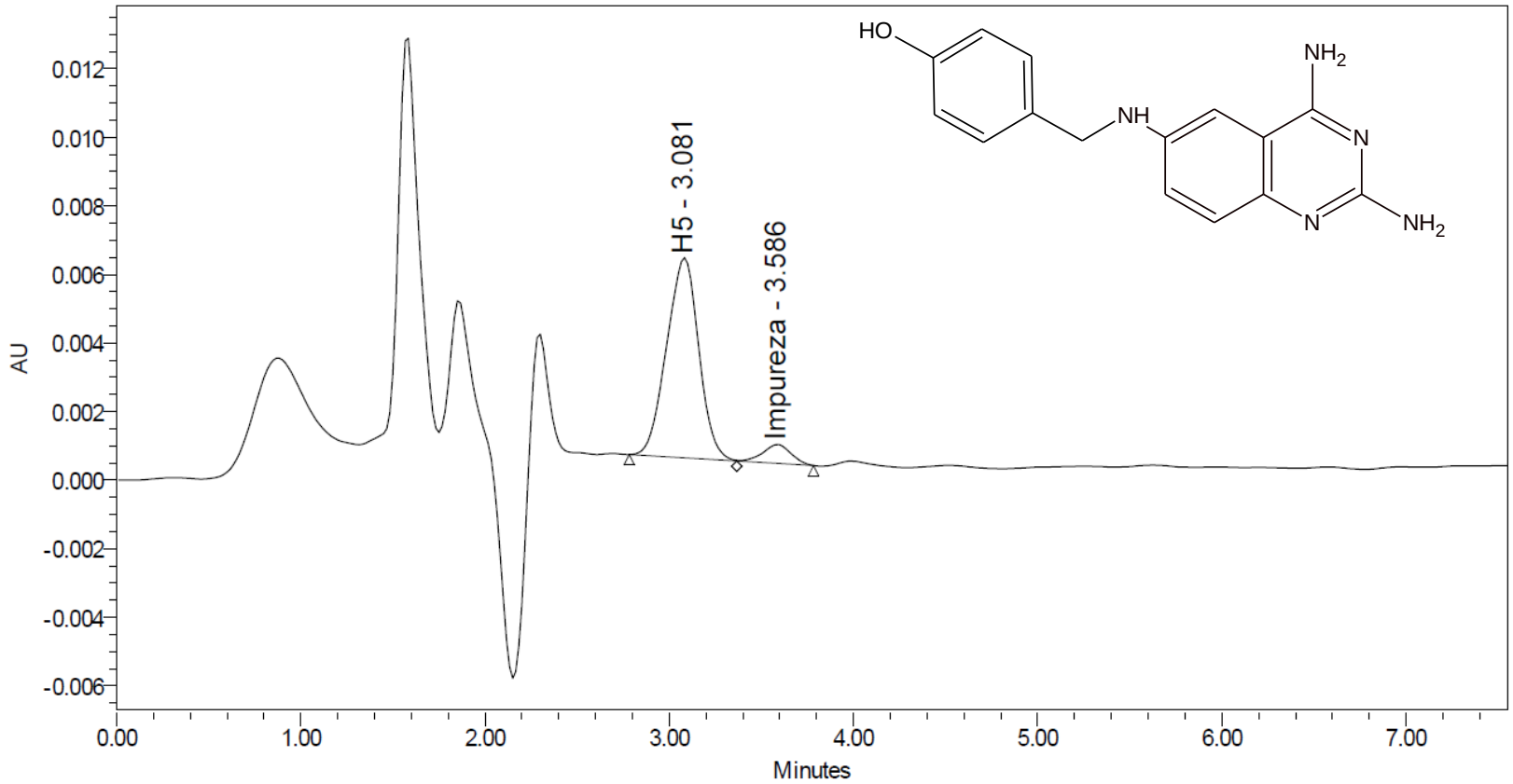

	Peak Name	RT	Area	% Area	Height	% Height	Units
1	H5	3.081	70827	92.36	5836	91.37	µg/mL
2	Impureza	3.586	5859	7.64	551	8.63	

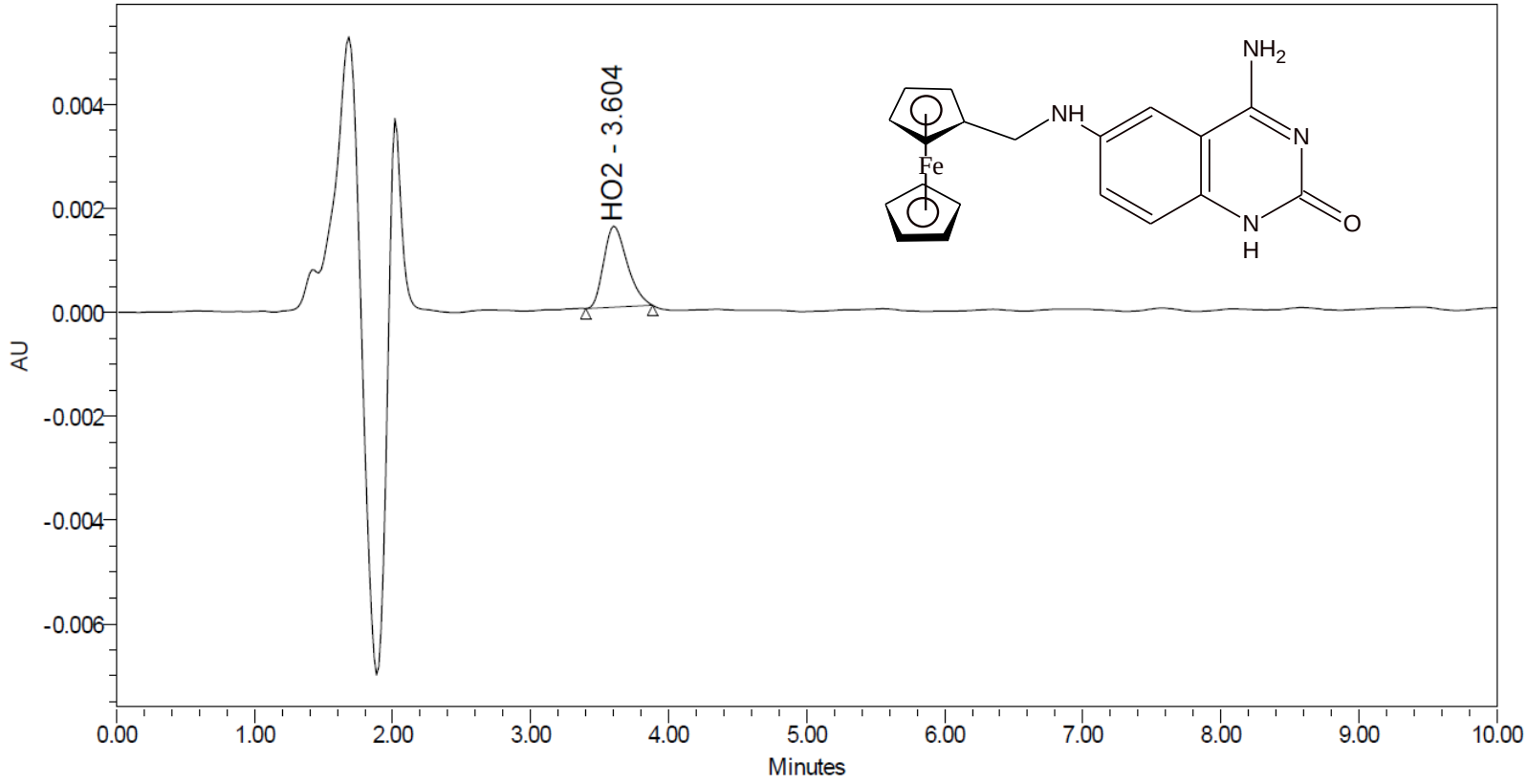

	Peak Name	RT	Area	% Area	Height	% Height	Units
1	HO2	3.604	18412	100.00	1560	100.00	µg/mL

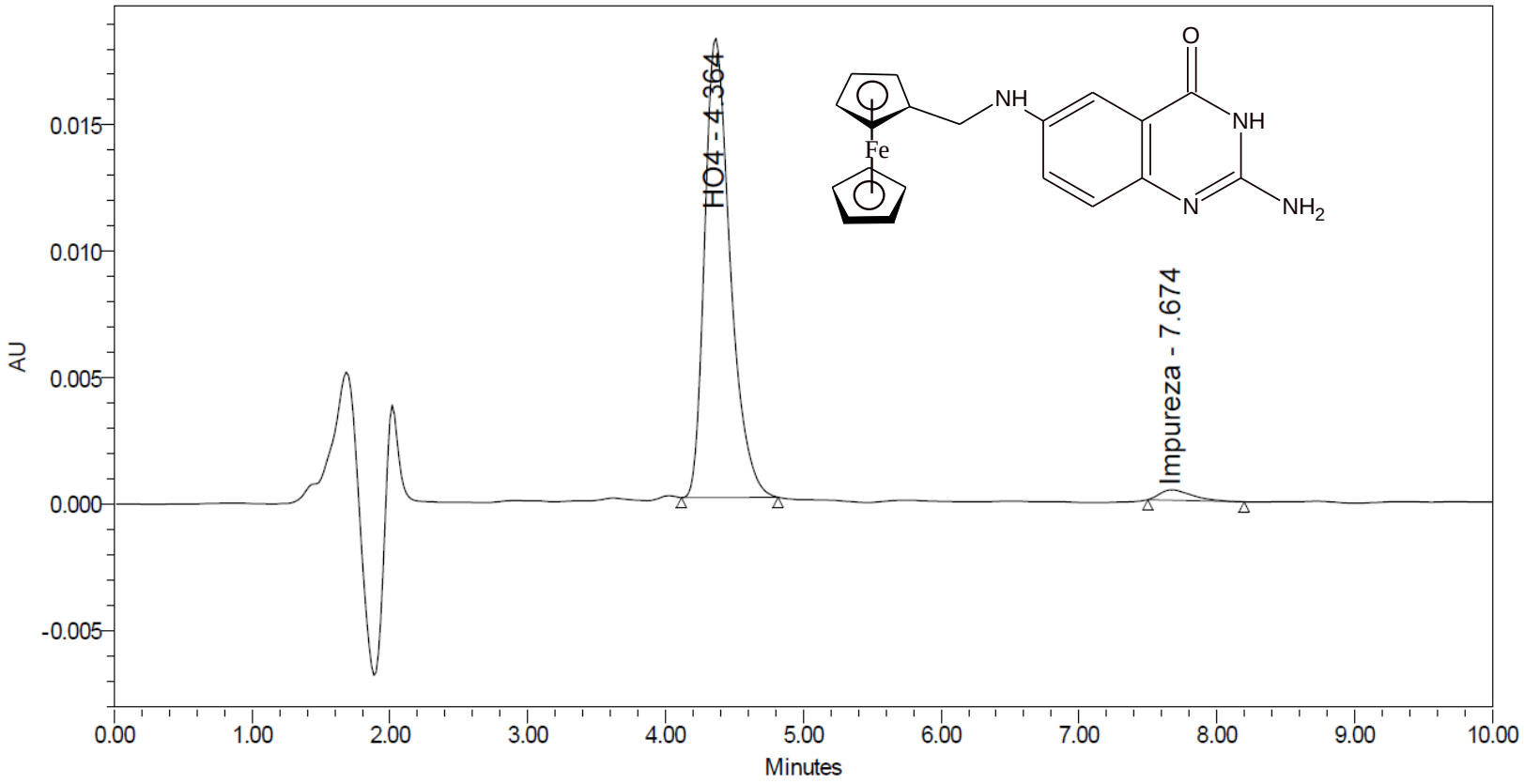

	Peak Name	RT	Area	% Area	Height	% Height	Units
1	HO4	4.364	234967	97.23	18175	97.79	µg/mL
2	Impureza	7.674	6685	2.77	411	2.21	